Available online at www.sciencedirect.com

SciVerse ScienceDirect

Geochimica et Cosmochimica Acta 75 (2011) 6094–6111

Geochimica et Cosmochimica Acta

www.elsevier.com/locate/gca

Benthic nitrogen cycling traversing the Peruvian oxygen minimum zone

L. Bohlen *, A.W. Dale, S. Sommer, T. Mosch, C. Hensen, A. Noffke, F. Scholz, K. Wallmann

Leibniz-Institut für Meereswissenschaften, IFM-GEOMAR, Gebäude Ostufer, Wischhofstr. 1–3, D-24148 Kiel, Germany

Received 8 November 2010; accepted in revised form 22 July 2011; available online 16 August 2011

Abstract

Benthic nitrogen (N) cycling was investigated at six stations along a transect traversing the Peruvian oxygen minimum zone (OMZ) at 11°S. An extensive dataset including porewater concentration profiles and in situ benthic fluxes of nitrate (NO_3^-), nitrite (NO_2^-) and ammonium (NH_4^+) was used to constrain a 1-D reaction-transport model designed to simulate and interpret the measured data at each station. Simulated rates of nitrification, denitrification, anammox and dissimilatory nitrate reduction to ammonium (DNRA) by filamentous large sulfur bacteria (e.g. *Beggiatoa* and *Thioploca*) were highly variable throughout the OMZ yet clear trends were discernible. On the shelf and upper slope (80–260 m water depth) where extensive areas of bacterial mats were present, DNRA dominated total N turnover ($\leqslant$2.9 mmol N m^{-2} d^{-1}) and accounted for $\geqslant$65% of $NO_3^- + NO_2^-$ uptake by the sediments from the bottom water. Nonetheless, these sediments did not represent a major sink for dissolved inorganic nitrogen ($DIN = NO_3^- + NO_2^- + NH_4^+$) since DNRA reduces NO_3^- and, potentially NO_2^-, to NH_4^+. Consequently, the shelf and upper slope sediments were recycling sites for DIN due to relatively low rates of denitrification and high rates of ammonium release from DNRA and ammonification of organic matter. This finding contrasts with the current opinion that sediments underlying OMZs are a strong sink for DIN. Only at greater water depths (300–1000 m) did the sediments become a net sink for DIN. Here, denitrification was the major process ($\leqslant$2 mmol N m^{-2} d^{-1}) and removed 55–73% of NO_3^- and NO_2^- taken up by the sediments, with DNRA and anammox accounting for the remaining fraction. Anammox was of minor importance on the shelf and upper slope yet contributed up to 62% to total N_2 production at the 1000 m station. The results indicate that the partitioning of oxidized N (NO_3^-, NO_2^-) into DNRA or denitrification is a key factor determining the role of marine sediments as DIN sinks or recycling sites. Consequently, high measured benthic uptake rates of oxidized N within OMZs do not necessarily indicate a loss of fixed N from the marine environment.

1. INTRODUCTION

As a limiting nutrient for biological productivity, nitrogen (N) occupies a central role in the biogeochemistry of the marine environment and exerts a significant influence on other elemental cycles, in particular carbon (Falkowski, 1997; Gruber, 2004). Bioavailable, or reactive, N in the ocean includes nitrate (NO_3^-), nitrite (NO_2^-) and ammonium (NH_4^+), whereas dinitrogen gas (N_2) is only accessible for nitrogen fixing bacteria. For the most part, the oceanic inventory of dissolved inorganic nitrogen ($DIN = NO_3^- + NO_2^- + NH_4^+$) depends on the balance between losses via denitrification (Codispoti et al., 2001; Gruber, 2004) and anammox (Dalsgaard et al., 2003; Kuypers et al., 2003) and gains through N_2 fixation.

Denitrification and anammox occur prominently in the water column in oxygen minimum zones (OMZs) and in anoxic marine sediments and together determine the extent

* Corresponding author. Tel.: +49 431 600 2267.
E-mail address: lbohlen@ifm-geomar.de (L. Bohlen).

0016-7037/$ - see front matter © 2011 Elsevier Ltd. All rights reserved.
doi:10.1016/j.gca.2011.08.010

of N deficit in these environments (Gruber and Sarmiento, 1997; Codispoti et al., 2001). An imbalance between sources and sinks of DIN may affect the intensity and potential growth of OMZs. For example, a loss of DIN from the water column due to denitrification or anammox may result in lower primary and export production and diminished oxygen (O_2) consumption rates in deeper water masses. Such a negative feedback could limit the ongoing spreading of OMZs (Oschlies et al., 2008; Stramma et al., 2008). However, benthic release of DIN potentially stimulates primary production and O_2 consumption in the water column, exacerbated by increased phosphorus fluxes from sediments underlying O_2-deficient waters (e.g. Ingall and Jahnke, 1994; Wallmann, 2010). This could drive the expansion of OMZs in a similar way to the biogeochemical feedback mechanisms driving Cretaceous ocean anoxic events (Van Cappellen and Ingall, 1994).

On a global scale marine sediments have been identified as fixed N sinks (e.g. Brandes and Devol, 2002), yet their source-sink function on regional scales is currently unclear (Fulweiler et al., 2007). Sediments underlying the hypoxic waters of upwelling regions are commonly perceived as sinks for DIN (Middelburg et al., 1996; Gruber and Sarmiento, 1997). Rate measurements are scarce, but those which do exist generally support this idea (Berelson et al., 1987; Devol and Christensen, 1993; Hartnett and Devol, 2003; Glud et al., 2009; Schwartz et al., 2009; Woulds et al., 2009). A recent study along 11°S within the Peruvian OMZ (Sommer et al., submitted for publication) showed the sediments were a sink for DIN on the continental slope at water depths with low dissolved O_2. However, on the shelf and upper slope the opposite was true. Here, mats of large vacuolated sulfur bacteria such as *Thioploca* and *Beggiatoa* (Mosch et al., 2010) were observed. These microorganisms internally store NO_3^- and, potentially NO_2^-, from the overlying seawater at millimolar concentrations (Fossing et al., 1995; Zopfi et al., 2001). The NO_3^- is used as an electron acceptor for sulfide oxidation in a process termed dissimilatory nitrate reduction to ammonium (DNRA), by which the microorganisms gain metabolic energy (e.g. Otte et al., 1999; Jørgensen and Nelson, 2004; Preisler et al., 2007). Large NH_4^+ effluxes have been measured on the shelf in these areas (Sommer et al., submitted for publication), and a rudimentary N mass balance by these workers indicates that a major proportion of the total $NO_3^- + NO_2^-$ uptake on the Peruvian shelf is channeled into DNRA rather than denitrification and anammox. DNRA by large sulfur bacteria has been identified as an important process in the N cycle and source of NH_4^+ to the porewater in organic matter-rich sediments on the continental shelf (Christensen et al., 2000; Otte et al., 1999; Graco et al., 2001; Dale et al., 2011). Critically, though, DNRA does not result in a net loss of DIN but instead recycles fixed N to the overlying water column in the form of NH_4^+. The significance of this process in the marine N budget is unknown.

The aim of this study is to investigate N cycling in the Peruvian OMZ sediments along 11°S and identify the major benthic N turnover processes under the changing redox conditions. We used a reaction-transport model constrained by measured in situ N fluxes and porewater geochemical profiles to explain the observed shift of the sediments as recycling sites for DIN on the shelf to DIN sinks down the continental slope. In contrast to previous modeling studies that simulated denitrification as a direct conversion of NO_3^- to N_2 (e.g. Middelburg et al., 1996; Van Cappellen and Wang, 1996), the role of the intermediate species, NO_2^-, is considered here owing to high concentrations in the water column on the shelf. We also focus on the importance of DNRA to N turnover since previous modeling studies suggest that it may dominate benthic sulfur and nitrogen cycling in suboxic upwelling regions as well as organic-rich costal sediments where sulfide accumulates in the porewater (e.g. Dale et al., 2009, 2011). Furthermore, because of the widespread occurrence of bacterial mats off southern Peru and Chile we expect this process to be significant (e.g. Gallardo, 1977; Fossing et al., 1995; Thamdrup and Canfield, 1996). To our knowledge this is the first modeling study to combine in situ flux data and numerical modeling to quantify DNRA and anammox along a redox gradient through fully anoxic to hypoxic bottom waters.

2. STUDY AREA

The Peruvian upwelling region forms part of the eastern boundary current system of the Eastern Tropical South Pacific. Alongshore winds engender offshore Ekman transport of surface waters which are replaced by O_2-poor, nutrient-rich equatorial subsurface waters of the Peru–Chile undercurrent (Fiedler and Talley, 2006; Silva et al., 2009). Upwelling stimulates high rates of primary productivity (1.8–3.6 g C m^{-2} d^{-1}, Reimers and Suess, 1983; Pennington et al., 2006; Fernández et al., 2009) and supports the development of an extensive OMZ (Fiedler and Talley, 2006; Silva et al., 2009). The upwelling intensity is seasonally variable and is most intense in austral winter and spring with interannual variability imposed by the El Niño Southern Oscillation (Morales et al., 1999; Kessler, 2006). The vertical extension of the OMZ reaches 700 m water depth off Peru (defined as $O_2 < 20$ μmol kg^{-1}; Fuenzalida et al., 2009), with an upper boundary that may be as shallow as 50 m (Morales et al., 1999) and deepen to ca. 200 m (e.g. Levin et al., 2002) during strong El Niño events.

The present study area at 11°S (Fig. 1) is located within the most intense coastal upwelling region and falls with the region of maximum primary productivity (Krissek et al., 1980; Pennington et al., 2006). This results in the formation of an upper-slope diatomaceous mud lens rich in organic-carbon and poor in carbonate between 10.5°S and 13.6°S (Zuta and Guillén, 1970; Krissek et al., 1980; Reimers and Suess, 1983). Preservation and burial of organic matter within the mud lens is supported by high sediment accumulation rates and diminished bottom current velocities (Suess et al., 1987). Sediment accumulates preferentially at water depths between 100 and 450 m and below 2000 m, whereas lower accumulation rates are found in the middle slope due to fluctuations in bottom current velocities (Reimers and Suess, 1983). At the time of sampling, the OMZ (defined here as $\leqslant 10$ μM O_2) extended from a water depth of ca.

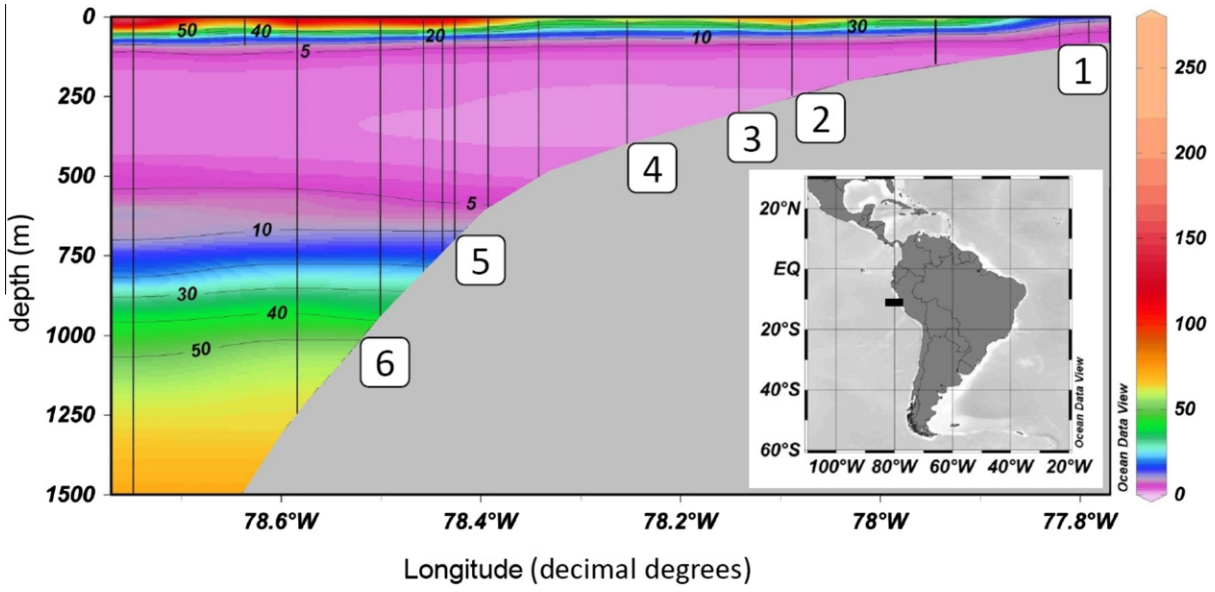

Fig. 1. Cross-section of oxygen concentrations (μM) on the shelf and slope of the Peruvian OMZ at 11°S. The vertical lines denote the CTD casts where O_2 measurements were made on cruise M77 leg 1. Station locations 1–6 for benthic studies are indicated. Note concentrations were ca. 45 μM at 10 m depth on the shelf, and that higher concentrations in the surface layers are not visible on this scale.

50–550 m (Fig. 1) and minimum bottom water O_2 concentrations were below the analytical detection limit (2 μM). In these anoxic areas, the surface sediments were characterized by extensive coverage by mats of large vacuolated sulfur bacteria such as *Thioploca* and *Beggiatoa* (Mosch et al., 2010).

3. MATERIALS AND METHODS

3.1. Sampling and geochemical analysis

Sediment cores were taken at 6 stations during two expeditions on RV Meteor (M77, leg 1 and 2) from October to December 2008 (late austral spring, high upwelling season) using multi-corers (MUC) and benthic lander deployments (BIGO). The latter were used to determine in situ fluxes of NH_4^+, NO_3^-, NO_2^- and, at the 2 deepest stations (5 and 6), total oxygen uptake (TOU). Complete details of the benthic flux measurements are provided by Sommer et al. (submitted for publication). Locations and water depths at the stations are listed in Table 1. With the exception of station 2, sediment samples were taken using both MUC and BIGO technologies. The retrieved cores were immediately transferred to a cool room onboard at 4 °C and processed within a few hours. Two parallel cores were taken for all MUC deployments. The first core was sub-sampled for redox sensitive constituents under anoxic conditions using an argon-filled glove bag. Sediment sections for porewater extraction were transferred into tubes pre-flushed with argon gas and subsequently centrifuged at max. 4500 G for 20 min. Prior to analysis, the supernatant porewater was filtered with 0.2 μm cellulose acetate Nuclepore® filters within the glove-bag. The centrifugation tubes with the remaining solid phase of the sediment were stored for further analysis

Table 1
Overview of stations and gear deployments.

Station No.	Core identifier	Date (2008)	Latitude (S)	Longitude (W)	Water depth (m)
1	M77-1 568 BIGO 5	November 15	11°00.02′	77°47.72′	85
	M77-1 543 MUC 52	November 12	10°59.99′	77°47.40′	78
2	M77-2 016 BIGO T6	November 29	10°59.80′	78°05.91′	259
3	M77-1 464 BIGO 1	November 5	11°00.00′	78°09.92′	315
	M77-1 449 MUC 19	November 3	11°00.01′	78°09.97′	319
4	M77-1 626 BIGO 3	November 20	11°00.02′	78°15.27′	397
	M77-1 481 MUC 33	November 6	11°00.00′	78°14.19′	376
5	M77-1 474 BIGO 2	November 5	11°00.01′	78°25.55′	695
	M77-1 459 MUC 25	November 4	11°00.03′	78°25.60′	697
6	M77-2 013 BIGO 6	November 29	10°59.82′	78°31.05′	978
	M77-1 549 MUC 53	November 13	10°59.81′	78°31.27′	1005

onshore. The second core was sub-sampled for porewater (i) without the glove-bag by squeezing 1–2 cm thick slices using a low pressure squeezer (argon at 2.5 bar) and filtering (0.2 μm) into recipient vessels, or (ii) anaerobically using rhizons®. For the BIGO deployments containing two chambers one core was taken from each. All BIGO cores were processed anaerobically with the glove bag as described above.

Samples for bottom water analysis were taken from the supernatant water of the sediment cores and from syringes attached to the outside of the benthic lander directly above the seabed.

Ammonium (NH_4^+), nitrite (NO_2^-), dissolved ferrous iron (Fe^{2+}), and total dissolved sulfide ($TH_2S \sim H_2S + HS^-$) were measured onboard using standard photometric techniques (Grasshoff et al., 1999). Aliquots of porewater were diluted with O_2-free artificial seawater prior to analysis where necessary. Porewater samples for Fe^{2+} analysis were treated with ascorbic acid directly after filtering (0.2 μm). Detection limits for NH_4^+, NO_2^- and TH_2S were 1 μM. Total alkalinity (TA) was determined onboard by direct titration of 1 ml porewater with 0.02 M HCl according to Ivanenkov and Lyakhin (1978) with an error of 0.05 meq l^{-1}. The titration method was calibrated using IAPSO seawater standard. Ion chromatography was used to determine nitrate (NO_3^-) and occasionally sulfate (SO_4^{2-}) in the onboard laboratory. Additional SO_4^{2-} analysis was performed onshore in porewater samples stored and transported in plastic vials. NO_3^- and SO_4^{2-} were measured with a detection limit of 1 and 10 μM, respectively and a relative error of 5% and 2%.

The solid phases were freeze-dried and analyzed for total particulate carbon, particulate organic nitrogen (PON) and total particulate sulfur (TPS) using a Carlo-Erba element analyzer (NA 1500). Particulate organic carbon (POC) content was determined on the residue after acidifying the sample with HCl (detection limit <0.1 wt% and relative error of 3%). Inorganic carbon was determined by weight difference. Additional sediment samples were embedded in epoxy resin for determination of gamma-ray excess ^{210}Pb activities at 46.5 keV on a low-background coaxial Ge(Li) detector.

Porosity was determined from the weight of the freeze-dried sediment and the water content. The volume fraction of the sediment was calculated using a dry sediment density of 2 g cm^{-3} (Böning et al., 2004). Further analytical details corresponding to the benthic lander deployments are described by Sommer et al. (submitted for publication).

3.2. Numerical modeling

3.2.1. Coupling reaction and transport

A 1-D numerical reaction-transport model was developed to simulate the biogeochemical cycles in the surface sediments at the 6 sampling stations along the 11°S transect. The length of the modeled domain, L, varied between 20 and 50 cm. In total 10 solutes were considered, including O_2, NO_3^-, NO_2^-, NH_4^+, N_2, TH_2S, SO_4^{2-}, Fe^{2+} as well as NO_3^- and NO_2^- stored in large sulfur bacteria ($NO_3^-{}_{bac}$, $NO_2^-{}_{bac}$). Solid species considered were POC, PON, adsorbed NH_4^+ ($NH_4^+{}_{ads}$), reactive iron oxide (FeOOH), sulfide-bound iron (FeII), TPS and excess ^{210}Pb. Solute and solid concentrations were modeled in units of mmol cm^{-3} of porewater and dry weight percent (wt%), respectively, except for $NH_4^+{}_{ads}$ (mmol g^{-1}). The modeled reaction network and rate expressions are described in Table 2 and the corresponding parameters are in Tables S1 and S2 in the Supplementary material.

Chemical species in the simulated sediment column were transported by advection due to sediment accumulation and compaction, molecular diffusion (for solutes), sediment mixing by fauna (bioturbation), non-local transport of solutes by fauna (bioirrigation) and non-local transport of $NO_3^-{}_{bac}$ and $NO_2^-{}_{bac}$ due to chemotaxis of large sulfur bacteria. Low Peclet numbers ($\ll 1$) over the length of the modeled sediment column (50 cm) illustrate that diffusion rather than advection is the dominant transport process for solutes below the irrigation layer (Boudreau, 1997). The following mass conservation equations were used to describe the temporal concentration change of solutes (C_i), $NO_3^-{}_{bac}$ and $NO_2^-{}_{bac}$ (C_b), and solids (C_j), due to transport and reaction:

$$\varphi\frac{\partial C_i}{\partial t} = \frac{\partial(\varphi(D_S + D_B)\frac{\partial C_i}{\partial x}}{\partial x} - \frac{\partial(\varphi v C_i)}{\partial x} + \varphi\alpha_i(C_{i(0)} - C_i) + \varphi\sum R_i \quad (1a)$$

$$\varphi\frac{\partial C_b}{\partial t} = \varphi\alpha_b(C_{b(0)} - C_b)\varphi\sum R_b \quad (1b)$$

$$\varphi(1-\varphi)\frac{\partial C_i}{\partial t} = \frac{\partial((1-\varphi)D_B\frac{\partial C_i}{\partial x})}{\partial x} - \frac{\partial((1-\varphi)wC_j)}{\partial x} + (1-\varphi)\sum R_j \quad (1c)$$

where t (year) is time, x (cm) is depth below the sediment–water interface, φ (dimensionless) is porosity, v (cm $year^{-1}$) is the burial velocity for solutes, w (cm $year^{-1}$) is the burial velocity for solids, D_S (cm^2 $year^{-1}$) is the tortuosity corrected molecular diffusion coefficient, D_B (cm^2 $year^{-1}$) is the bioturbation coefficient, α_i ($year^{-1}$) is the bioirrigation coefficient, α_b ($year^{-1}$) is the coefficient for non-local NO_3^- and NO_2^- transport by bacteria, $C_{i(0)}$ and $C_{b(0)}$ are the concentrations of solutes and NO_3^- or NO_2^- in bacteria at the sediment–water interface, respectively, and ΣR is the sum concentration change due to chemical reactions. $NO_3^-{}_{bac}$ and $NO_2^-{}_{bac}$ were assumed to be confined to the vacuoles and thus not transported by diffusion or burial. In these equations φ, D_S, D_B, v, w, α_i, α_b are depth-dependent and explained in more detail in the Supplementary material.

The model was run to steady-state ($\partial C/\partial t = 0$), although we are aware that the shelf is a more transient environment than the deeper slope settings. For example, an increase in POC accumulation rates began around 1820 AD (Gutiérrez et al., 2009) and the shelf bottom waters were renewed and ventilated in 1993 and 1997/98 in response to El Niño events (Gutiérrez et al., 2008). Nonetheless, we argue that (i) the relatively slow change in solid accumulation rates beginning ca. 200 years ago allows the solutes in the upper 50 cm to approach dynamic equilibrium with regard to POM mineralization, and (ii) the 13 years period since the last major oxygenation event on the shelf is sufficiently long for the N fluxes and turnover rates in the surface layers impacted by microbial mats (<10 cm) also to have reached quasi-steady state conditions. In support of this argument, diffusion time-scales calculated from the modified Einstein–

Table 2
Reaction network used in the model. Model parameters are listed in Tables S1 and S2 in the Supplementary material.

Process	Stoichiometry	Rate expression [a]
R_1	$(CH_2O)(NH_3)_{rNC} + O_2 \rightarrow (1 - r_{NC})CO_2 + (r_{NC})HCO_3^- + r_{NC}NH_4^+(1 - r_{NC})H_2O$	$R_{POC} \times \frac{[O_2]}{[O_2]+K_1}$
R_2	$(CH_2O)(NH_3)_{rNC} + 2NO_3^- \rightarrow 2NO_2^- + (1 - r_{NC})CO_2 + (r_{NC})HCO_3^- + r_{NC}NH_4^+ + (1 - r_{NC})H_2O$	$R_{POC} \times \frac{[NO_3^-]}{[NO_3^-]+K_2} \times \frac{K_3}{[NO_2^-]+K_3} \times \frac{K_1}{[O_2]+K_1}$
R_3	$(CH_2O)(NH_3)_{rNC} + 4/3NO_2^- + (1/3 + r_{NC})CO_2 \rightarrow 2/3N_2 + (4/3 + r_{NC})HCO_3^- + r_{NC}NH_4^+ + (1/3 - r_{NC})H_2O$	$R_{POC} \times \frac{[NO_2^-]}{[NO_2^-]+K_3} \times \frac{K_1}{[O_2]+K_1}$
R_4	$(CH_2O)(NH_3)_{rNC} + 4FeOOH + (7 + r_{NC})CO_2 + (1 + r_{NC})H_2O \rightarrow 4Fe^{2+} + (8 + r_{NC})HCO_3^- + r_{NC}NH_4^+$	$R_{POC} \times \frac{[FeOOH]}{[FeOOH]+K_4} \times \frac{K_2}{[NO_3^-]+K_2} \times \frac{K_3}{[NO_2^-]+K_3} \times \frac{K_1}{[O_2]+K_1}$
R_5	$(CH_2O)(NH_3)_{rNC} + 0.5SO_4^{2-} + (r_{NC})CO_2 + (r_{NC})H_2O \rightarrow 0.5H_2S + (1 + r_{NC})HCO_3^- + r_{NC}NH_4^+$	$R_{POC} \times \frac{K_4}{[FeOOH]+K_4} \times \frac{K_2}{[NO_3^-]+K_2} \times \frac{K_3}{[NO_2^-]+K_3} \times \frac{K_1}{[O_2]+K_1}$
R_6	$NH_4^+ + 3/2\ O_2 + 2\ HCO_3^- \rightarrow NO_2^- + 3\ H_2O + 2\ CO_2$	$k_6 \times [O_2] \times [NH_4^+]$
R_7	$NO_2^- + 1/2\ O_2 \rightarrow NO_3^-$	$k_7 \times [O_2] \times [NO_2^-]$
R_8	$NH_4^+ + NO_2^- \rightarrow 2\ N_2 + 2\ H_2O$	$k_8 \times [NO_2^-] \times [NH_4^+]$
R_9	$HS^- + NO_3^- + CO_2 + 2\ H_2O \rightarrow SO_4^{2-} + NH_4^+ + HCO_3^-$	$k_9 \times [NO_3^-{}_{bac}] \times [TH_2S]$
R_{10}	$HS^- + 4/3\ NO_2^- + 5/3\ CO_2 + 9/3\ H_2O \rightarrow SO_4^{2-} + 4/3\ NH_4^+ + 5/3\ HCO_3^-$	$k_{10} \times [NO_2^-{}_{bac}] \times [TH_2S]$
R_{11}	$NH_4^+ \leftrightarrow NH_4^+{}_{ads}$	$k_{11} \times (1 - [NH_4^+{}_{ads}]/([NH_4^+] \times K_{NH4}))$ [b]
R_{12}	$Fe^{2+} + 1/4\ O_2 + 2\ HCO_3^- \rightarrow FeOOH + 2\ CO_2 + 1/2\ H_2O$	$k_{12} \times [O_2] \times [Fe^{2+}]$
R_{13}	$HS^- + 2\ O_2 + HCO_3^- \rightarrow SO_4^{2-} + CO_2 + H_2O$	$k_{13} \times [O_2] \times [TH_2S]$
R_{14}	$Fe^{2+} + 1/5\ NO_3^- + 9/5\ HCO_3^- \rightarrow FeOOH + 1/10\ N_2 + 9/5\ CO_2 + 2/5\ H_2O$	$k_{14} \times [NO_3^-] \times [Fe^{2+}]$

[a] The factor $f_i = \varphi/(1 - \varphi) \times M_i/(10 \times ds)$ where M_i is the molecular mass of species i (g mol^{-1}), was used to convert between dissolved species in units of mmol cm^{-3} of porewater and solid phase species in dry weight percent (wt%).

[b] The factor $\varphi/((1 - \varphi) \times ds)$ was used to convert between dissolved and adsorbed NH_4^+ (mmol g^{-1}).

Smoluchowski equation (Jørgensen et al., 2004) for a typical solute are on the order of 10 and 1 year for the upper 50 and 10 cm of the sediment, respectively.

3.2.2. Reaction network

The biogeochemical reactions considered (Table 2) were driven by the degradation of particulate organic matter (POM), defined chemically as $(CH_2O)(NH_3)_{rNC}$ where r_{NC} is the molar ratio of N:C. POM was degraded by aerobic respiration (R_1), denitrification (R_2, R_3), iron oxide reduction (R_4) and sulfate reduction (R_5). Manganese oxide reduction and methanogenesis were neglected because measured dissolved and solid Mn concentrations were low (<1 μM and <0.05 wt%, respectively) and SO_4^{2-} was never exhausted over the modeled sediment layer. The organic nitrogen in POM was liberated as NH_4^+ during mineralization rather than being directly coupled to nitrification (Van Cappellen and Wang, 1996) since these processes are mediated by different groups of microorganisms. The relative rates of each POM degradation pathway were determined using Michaelis–Menten kinetics (e.g. Boudreau, 1996), where the electron acceptors O_2, NO_3^-, NO_2^-, FeOOH and SO_4^{2-} were used sequentially in this order until their concentrations decreased to limiting levels defined by different half saturation constants (K) for each electron acceptor. Bimolecular rate laws were used for all secondary redox reactions (Van Cappellen and Wang, 1996).

TA was not modeled explicitly and was calculated from the major ion concentrations at each depth (x) relative to their concentrations at the sediment–water interface

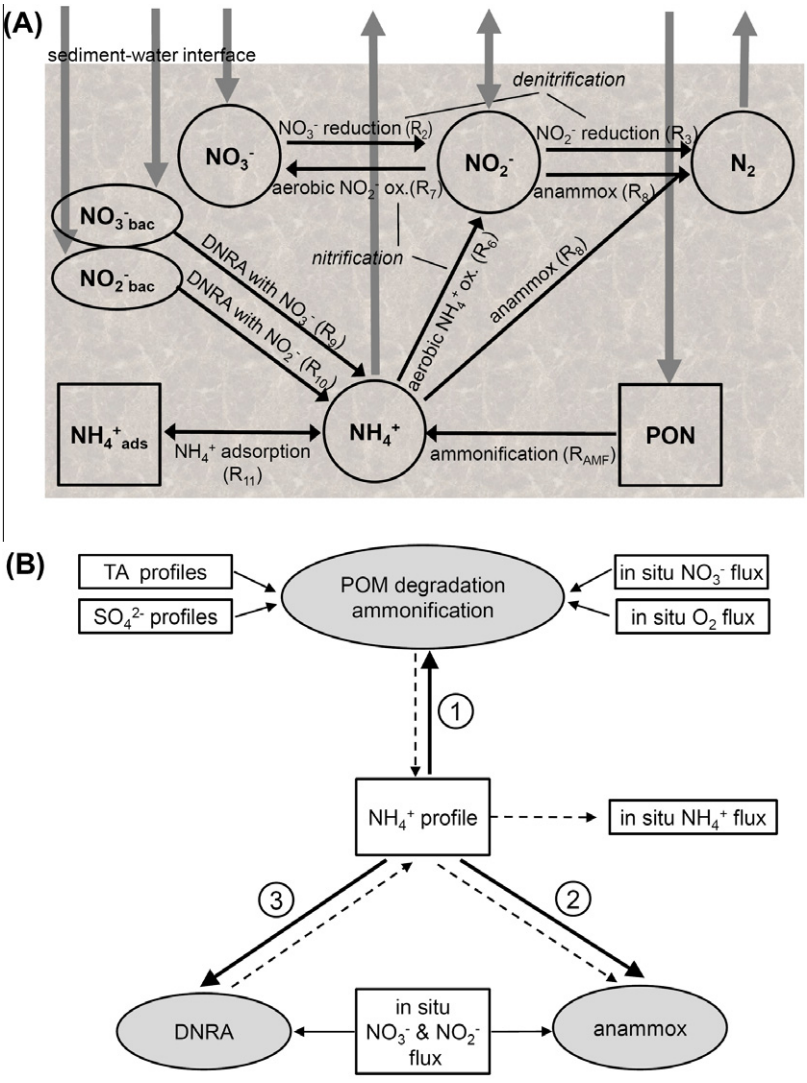

Fig. 2. (A) The N cycle considered in the model. Circles and squares denote porewater and solid species, respectively, and the ellipses denote filamentous sulfur bacteria. Reactions simulated with the model are shown with black arrows and the fluxes across the sediment–water interface are shown by dashed arrows. The stoichiometry of the reactions is listed in Table 2. (B) Procedure used to constrain the rates of POM degradation, DNRA and anammox described in the text (steps #1–3). Rectangles denote measured data and ellipses denote biogeochemical processes. Black arrows show constraints described in the text and the dashed arrows denote sources and sinks of NH_4^+. The rate constants for NH_4^+ oxidation and adsorption were fixed and these processes are not shown.

($x = 0$) using the explicit conservative expression for TA (Wolf-Gladrow et al., 2007):

$$\begin{aligned} TA(x) = TA(0) &- (NO_3^-(x) - NO_3^-(0)) + (NH_4^+(x) \\ &- NH_4^+(0)) - 2 \times (SO_4^{2-}(x) - SO_4^{2-}(0)) \\ &- (NO_2^-(x) - NO_2^-(0)) + 2 \times (Fe^{2+}(x) \\ &- Fe^{2+}(0)) \end{aligned} \quad (2)$$

A schematic overview of the modeled N cycle is shown in Fig. 2A. Organic nitrogen was released as NH_4^+ during POM mineralization (ammonification, R_{AMF}). Canonical denitrification was modeled as a two-step process (R_2, R_3) with NO_2^- as an intermediate species. The kinetics of this process was formulated such that POM degradation via NO_3^- was inhibited by the accumulation of NO_2^- (Table 2), i.e. POM was preferentially degraded by NO_2^-. We took this approach since denitrifying organisms harvest a greater amount of catabolic energy during the reduction of NO_2^- to N_2 compared to NO_3^- reduction to NO_2^- under standard conditions (Thauer et al., 1977; Lam and Kuypers, 2011). Similarly, nitrification, was described as the stepwise oxidation of NH_4^+ to NO_2^- followed by NO_2^- to NO_3^- (R_6, R_7). In our model, therefore, NO_2^- was allowed to accumulate in the porewater, thus permitting competition between denitrification (R_3), nitrification (R_7) and anammox (R_8) for NO_2^-. The latter process produces N_2 gas from NO_2^- and NH_4^+ (Thamdrup and Dalsgaard, 2002; Dalsgaard et al., 2005) and is an important pathway of nitrogen loss in the marine environment (Thamdrup and Dalsgaard, 2002; Dalsgaard et al., 2005; Hamersley et al., 2007; Lam et al., 2009). Denitrification coupled to Fe^{2+} oxidation (Straub et al., 1996) was also considered to compete with canonical denitrification for NO_3^-. However, simulations (not shown) revealed that this process was of minor importance (contributing <0.1% to total N_2 production) and will thus not be discussed further. In what follows, the term 'denitrification' applies to canonical denitrification (i.e. R_2 followed by R_3) rather than anammox (R_8).

At station 1, where bottom water NO_2^- was elevated and NO_3^- concentrations were low (Table 3), DNRA was allowed to proceed using both NO_3^- (R_9) and NO_2^- (R_{10}) as electron acceptors. In support of this assumption, Zopfi et al. (2001) observed positive chemotaxis of *Thioploca* toward NO_2^-, suggesting a direct response of large sulfur bacteria to NO_2^-. At the other stations where seawater NO_2^- concentrations were <3 μM (Table 3), NO_3^- was considered to be the only available electron acceptor for DNRA.

NH_4^+ was allowed to adsorb onto sediment particles (R_{11}). Although this process is more correctly described as a dynamic equilibrium between dissolved and adsorbed NH_4^+ defined by an empirical equilibrium constant, K_{NH4} (Morse and Morin, 2005), it was simulated as a kinetic process whose rate is partially determined by the departure from equilibrium (Table 2). The rate constant was set to sufficiently large values to ensure that dynamic equilibrium between dissolved and adsorbed ammonium was always maintained (Wallmann et al., 2008).

Although iron and sulfur cycling were included in the reaction network through their coupling with the nitrogen cycle, only the most relevant reactions were considered. Labile FeOOH can undergo dissimilatory iron reduction (R_4) producing Fe^{2+}. Subsequently, Fe^{2+} may be either oxidized by O_2 (Table 2) to FeOOH or be precipitated as sedimentary iron sulfide minerals. Dissolved sulfide may be either oxidized aerobically or anaerobically (i.e. by DNRA) or be precipitated into particulate iron minerals or incorporated in organic matter. The iron and sulfide precipitation reactions are not described by explicit reactions.

Table 3
Model boundary conditions at the sediment–water interface.

	Station 1	Station 2	Station 3	Station 4	Station 5	Station 6
O_2 [μM]	0[a]	0[a]	0[a]	0[a]	8	40
NO_3^- [μM]	3.1	15	26	33	40	40
NO_2^- [μM]	11.5	2.3	2.85	0.48	0.25	0.27
NH_4^+ [μM]	0.45	1.1	1.14	0.56	0.02	0
SO_4^{2-} [mM]	29	29	29	29	29	29
TH_2S [μM]	0	0	0	0	0	0
Fe^{2+} [μM]	0	0	0	0	0	0
TA [mM]	1.96	2.38	2.23	2.5	2.28	2.35
N_2 [μM] [b]	489	498	501	532	553	574
$NO_3^-{}_{bac}$ [μM]	119 [c]	100 [d]	102 [c]	33[c]	–	–
$NO_2^-{}_{bac}$ [μM]	12	–	–	–	–	–
POC (mmol m^{-2} d^{-1}) [e]	14.3	11.8	9.4	6.9	9.1	5.9
PON (mmol m^{-2} d^{-1}) [f]	1.63	1.10	0.99	0.80	0.9	0.53
TPS (mmol m^{-2} d^{-1})	0	0	0	0	0	0
FeOOH (mmol m^{-2} d^{-1})	1.73	0.12	0.11	0.15	0.49	0.46

[a] Below analytical detection limit (<2 μM).
[b] Calculated according to Hamme and Emerson (2004) using site-specific temperature (Table S2) and a salinity of 35.
[c] Estimated from porewater NO_3^- concentrations after sediment squeezing.
[d] Estimated from values at stations 1 and 3.
[e] Determined from the mass balance for upper 10 cm (Sommer et al., submitted for publication).
[f] Calculated from the POC flux applying measured N:C values (r_{NC}, Table S2).

Instead, the rates of these processes were estimated from fitting appropriate functions to the Fe^{2+} and TH_2S profiles. This procedure is described in the Supplementary material.

3.2.3. Constraints on the rates of N cycling

Rates of benthic N turnover processes at each station were not measured directly using, for example, ^{15}N labeling studies but were instead indirectly estimated by applying the numerical model to the measured porewater profiles and benthic fluxes. The procedure is outlined graphically in Fig. 2B and described below.

An initial guess for the rate of POM degradation at each station was made from the measured NH_4^+ profiles. At steady state, Eq. (1a) shows that the net accumulation of NH_4^+ at each depth will be zero due to a balancing of the transport and reaction terms. In this case, the sum of reactions involving NH_4^+, $\Sigma R_{NH4}(x)$, can be expressed as:

$$\Sigma R_{NH4}(x) = R_{AMF}(x) - R_6(x) - R_8(x) + R_9(x) + (4/3 \times R_{10}(x)) - R_{11}(x) \quad (3)$$

where $R_{AMF}(x)$ is the rate of NH_4^+ production during organic matter degradation and the other reactions are listed in Table 2. Typically, the NH_4^+ data would be simulated by adjusting the rate constants in the individual reactions expression in the above equation. In our approach, however, a continuous function was fit through the measured NH_4^+ concentrations to obtain a profile of observed NH_4^+ ($NH_4^+{}_{OBS}(x)$). The following fitting function was then used to describe $\Sigma R_{NH4}(x)$:

$$\Sigma R_{NH4}(x) = k_{fit} \times (NH_{4\,OBS}^+(x) - NH_4^+(x)) \quad (4)$$

where $NH_4^+(x)$ is the modeled NH_4^+ profile and k_{fit} ($year^{-1}$) is a kinetic constant. k_{fit} was prescribed a high value to ensure that the modeled concentrations were maintained close to the measured values. With this approach, the observed NH_4^+ concentrations constitute an external forcing to the model which allows $\Sigma R_{NH4}(x)$ to be quantified without explicitly specifying a kinetic rate expression for ammonium production during organic matter degradation. The rate of ammonification was then determined from Eqs. (3) and (4):

$$R_{AMF}(x) = k_{fit} \times (NH_{4\,OBS}^+(x) - NH_4^+(x)) + R_6(x) + R_8(x) - R_9(x) - (4/3 \times R_{10}(x)) + R_{11}(x) \quad (5)$$

Consequently, the rate of POC mineralization (R_{POC}) was estimated from $R_{AMF}(x)$ by the following expression:

$$R_{POC}(x) = R_{AMF}(x)/r_{NC} \quad (6)$$

The determination of $R_{AMF}(x)$ thus required knowledge of the rates of nitrification (R_6), anammox (R_8), DNRA (R_9, R_{10}) and NH_4^+ adsorption (R_{11}). The rates of nitrification and NH_4^+ adsorption were parameterized using constants whose values were invariable across the transect (Table S1 in the Supplementary material). The rate constants for anammox and DNRA (Table S2) were variable and adjusted to fit the measured fluxes. To begin with, the rates of anammox and DNRA were initially set to zero which means that ammonification is the only unknown process affecting NH_4^+ concentrations. If this were correct, the modeled NH_4^+, TA and SO_4^{2-} profiles and DIN fluxes would be consistent with the measured data (Fig. 2B, step #1). However, this was not the case for any station, which indicates the occurrence of DNRA and/or anammox (Fig. 2B, steps #2 and #3). Furthermore, the flux of NO_3^- and/or NO_2^- into the sediment was underestimated at all stations when anammox and DNRA were not considered. This deficit must then be due to one or both of these processes since the rate of denitrification (R_2, R_3) is indirectly imposed by R_{POC} (Eq. (6)).

Rates of DNRA and anammox at the individual stations were constrained according to three criteria. Firstly, where the initial model simulation underestimated both NO_3^- and/or NO_2^- uptake into the sediment and POM degradation (indicated by too low TA and too high SO_4^{2-} concentrations), anammox was assumed to take place (Fig. 2B, step #2). Anammox consumes NO_2^- and NH_4^+, thus leading to higher rates of POM degradation in order to maintain the fit to the observed NH_4^+ data and, consequently, enhanced accumulation of TA and consumption of SO_4^{2-} (Eq. (5)). If the measured benthic fluxes and concentrations profiles could be simulated by only considering anammox, DNRA was assumed not to occur. Note that for the above criteria, increasing the rate of DNRA instead of anammox would slow down, rather than enhance, the rate of POM degradation since more NH_4^+ would be produced, ultimately leading to a greater misfit with the TA and SO_4^{2-} data.

Secondly, where the initial model simulation underestimated NO_3^- and/or NO_2^- uptake and overestimated POM mineralization (indicated by too high TA and too low SO_4^{2-} concentrations), DNRA was assumed to take place (Fig. 2B, step #3). As mentioned, DNRA enhances NO_3^- (and NO_2^-) uptake into the sediment and produces NH_4^+, leading to a decrease of POM degradation and TA concentrations through Eq. (5). If the model adequately simulated the measured benthic N fluxes and the porewater profiles with DNRA only, anammox was assumed not to occur.

Finally, if the uptake of NO_3^- and/or NO_2^- into the sediment was underestimated in the model even after DNRA was considered, the remaining NO_3^- and/or NO_2^- uptake was attributed to anammox. This systematic approach, therefore, allows for the occurrence of only DNRA and anammox or, if necessary, both processes together to explain the benthic fluxes.

3.2.4. Boundary conditions and model solution

Boundary conditions for each species at the top and the bottom of the modeled sediment layer were required to solve the differential equations (Eq. 1). At the sediment–water interface fixed concentrations were imposed for solutes (Dirichlet type) and fixed fluxes for solids (Robin type). Solute concentrations were assigned measured bottom water values where available (Table 3). Concentrations of NO_3^- and NO_2^- in large sulfur bacteria were not measured but were estimated from the porewater NO_3^- concentrations in squeezed sediment samples in the uppermost sediment layer which yielded higher NO_3^- concentrations compared to centrifuged samples or rhizon extractions (see Section 4.1). This assumes that squeezing destroyed the bacterial cells and released the nitrate stored in their

vacuoles (Thamdrup and Canfield, 1996). The imposed upper boundary for $NO_3^-{}_{bac}$ and $NO_2^-{}_{bac}$ should be regarded as minimum estimates since repeated freezing and thawing the sediment is required to fully destroy the cells and liberate the intracellular fluid (Dale et al., 2009).

POC fluxes to the sediment–water interface were constrained from a simple mass balance of the sediment at each station developed by Sommer et al. (submitted for publication). The range of the organic carbon flux used in this model (6–14 mmol m^{-2} d^{-1}, Table 3) compares very well to the TOC flux off Callao at 12°S (~3–14 mmol m^{-2} d^{-1}; Sifeddine et al., 2008) and the organic carbon flux reported by Henrichs and Farrington (1984) at 15°S (9–16 mmol m^{-2} d^{-1}). PON fluxes were calculated using the measured C:N ratio in the top layer of sediment and the POC flux. Reactive FeOOH flux was calculated from the Al deposition rate (derived from the ^{210}Pb measurements) and the Fe/Al ratio of 0.47 in andesitic volcanic rocks (Sarbas and Nohl, 2009) forming the local drainage area. Moreover, we assumed that only 50% of the total iron reaching the seafloor was reactive in the surface layers (Poulton and Raiswell, 2002). Particulate sulfur fluxes at the top boundary were set to zero. The upper boundary for $NH_4^+{}_{ads}$ was implicitly given by the upper boundary concentration of NH_4^+ and the apparent equilibrium coefficient for adsorption.

Solid species were prescribed zero-gradient (Neumann type) conditions at the lower boundary ($x = L$ cm) at all stations. A similar condition was also prescribed for solutes at stations 5 and 6 because the concentrations were invariable at the depth of the lower model boundary. At stations 1–4 distinct concentrations changes at the bottom boundary were observed, and here a constant gradient condition was imposed:

$$\left.\frac{\delta C_i}{\delta x}\right|_{n=100} = 0.95 \times \left.\frac{\delta C_i}{\delta x}\right|_{n=99} \quad (7)$$

where n refers to a layer (0–100) in the discretized grid space. This gradient resembles the near-linear measured concentration profiles of TA and SO_4^{2-} close to the bottom boundary. For NH_4^+, whose concentration was fit to the observed data, the gradient was set to that of the fitting function at the bottom boundary.

Finite differences and the method of lines were used to solve the set of coupled partial differential equations (Boudreau, 1996). A central differences scheme was applied over an uneven grid for diffusion, bioturbation, and advection in the bioturbated layer whereas upward differences were used for advective transport below the bioturbated zone. Depth intervals increased with sediment depth to a maximum resolution of 1 cm. The set of coupled ordinary differential equations was solved using the numerical solver NDSolve in MATHEMATICA 7.0. Mass conservation of the model was >99% and a typical steady-state simulation was completed within 5 min on a personal computer (Intel Core 2 Duo processor).

4. RESULTS AND DISCUSSION

4.1. Sediment geochemistry and POM degradation

Porewater NH_4^+, NO_3^-, TH_2S, SO_4^{2-} and TA profiles for all stations are shown in Fig. 3. Maximum TA and NH_4^+ concentrations of 14 meq l^{-1} and 1.2 mM, respectively, were observed at the base of the core at the shallowest site (station 1). Steep NH_4^+ and TA concentration gradients at the sediment–water interface and a strong convex curvature of the profiles indicate high rates of POM mineralization in the surface layers on the shelf. For the Peru upwelling region at 12°S (183 m water depth), higher concentrations of about 25 meq l^{-1} TA and 2.8 mM NH_4^+ have been reported (Froelich et al., 1988). Further south at 15°S, NH_4^+ concentrations >3 mM at 60 cm were measured at a site at 245 m water depth (Rowe and Howarth, 1985). The rates of POM mineralization on the shelf at 11°S are thus on the low side of previous reports. However, the NH_4^+ concentrations were elevated compared to other high productivity OMZ regions such as offshore central Chile (<0.8 mM; Thamdrup and Canfield, 1996) and the Pakistan margin (<0.3 mM; Woulds et al., 2009). The decrease in NH_4^+ and TA concentration gradients from station 1 to station 6 (Fig. 3) allude to a decrease in POM degradation rates with increasing water depth. This is confirmed by the SO_4^{2-} concentration data which is progressively less depleted down slope.

These qualitative trends were supported by quantitative modeling of POC degradation rates (Table 4). Total mineralization rates decreased from 8.23 mmol C m^{-2} d^{-1} on the shelf to 1.74 mmol C m^{-2} d^{-1} at station 5 on the slope. At stations 1 and 2 sulfate reduction was by far the dominant POC degradation pathway (up to 80% of total) and became relatively less important with increasing water depth. Empirical data sets predict that sulfate reduction accounts for ca. 70% of organic carbon mineralization on the shelf (0–200 m) whereas aerobic respiration contributes only 10% (Burdige, 2006). Based on these data, it can be inferred that sulfate reduction consumes the fraction of POM normally respired aerobically. Nonetheless, the modeled sulfate reduction rates (<6.6 mmol C m^{-2} d^{-1}) were a factor of 7–20 lower than measured rates from studies on the shelf off Peru and Chile (Fossing et al., 1995; Ferdelman et al., 1997), yet our derived total POC degradation rates were too low to support such high sulfate reduction rates except at station 1. Böning et al. (2004) reported sulfate reduction rates for 14 stations on the Peruvian shelf of which only two were >3.9 mmol S m^{-2} d^{-1} or twice this value for in terms of carbon mineralization. Furthermore, sulfate reduction rates equivalent to ca 2.4 and 1.2 mmol C m^{-2} d^{-1} were reported for 36°S and 23°S, respectively (Niggemann et al., 2007). Clearly, there is pronounced spatial heterogeneity in the total organic matter degradation rate in the OMZ off Peru and Chile.

The low total mineralization rates at the deep stations 5 and 6 are markedly higher than the measured TOU of ca. 0.5 and 1.5 mmol O_2 m^{-2} d^{-1}, respectively (Fig. 4). This indicates that a large fraction of the reduced metabolites (e.g. NH_4^+, TH_2S) escape oxidation and are either buried or transported to the water column. The model underestimates the TOU by up to a factor of 2 and 3 at station 5 and 6, respectively. The reason for this discrepancy is not clear, but may be due to respiration by fauna or oxidation of reduced species in the chamber water rather than the sediments (Sommer et al., 2010).

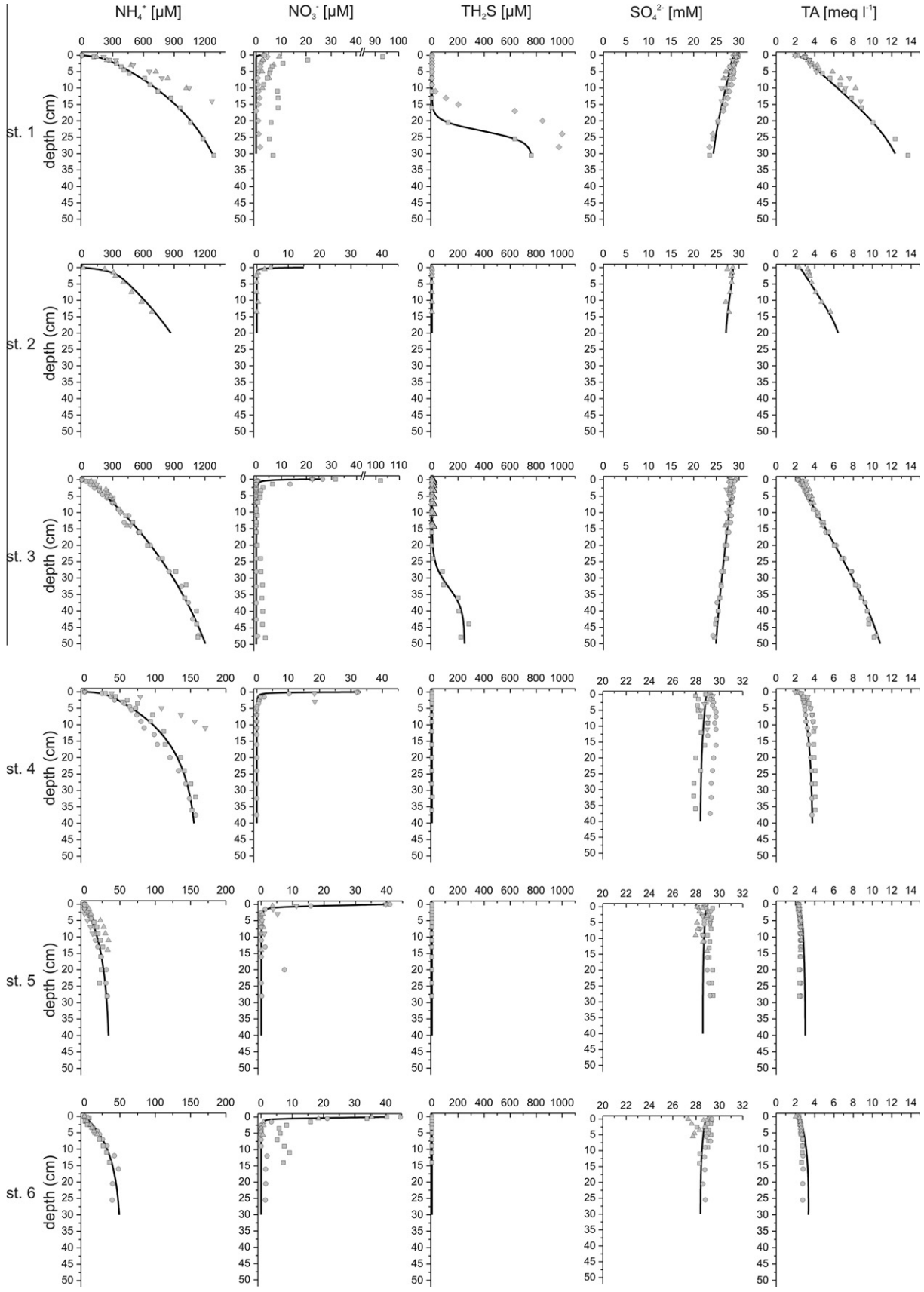

Fig. 3. Modeled (lines) and measured (symbols) porewater concentration profiles of NH_4^+, NO_3^-, TH_2S, SO_4^{2-} and TA at stations 1 to 6. Symbols denote the following porewater subsampling methods: circles = MUC, glove-bag; squares = MUC, porewater squeezer; diamonds = MUC, rhizons; triangles = BIGO, glove-bag. NH_4^+ concentrations were fitted using the procedure described in the text. Note the different concentration scales for NH_4^+ and NO_3^- between stations.

Table 4
POC degradation rates (mmol C m^{-2} d^{-1}) across the transect rounded to two decimal places. Percentages of the total POC degradation rate used by each electron acceptor rounded to the nearest integer are given in parenthesis. A 20% uncertainty is assigned to the rates (see Section 4.4).

Process	Station 1	Station 2	Station 3	Station 4	Station 5	Station 6
R_1 (O_2)	0 (0)	0 (0)	0 (0)	0 (0)	0.23 (14)	0.59 (28)
R_2 (NO_3^-)	0.17 (2)	0.65 (8)	0.95 (16)	0.91 (23)	0.28 (16)	0.18 (8)
R_3 (NO_2^-)	1.08 (13)	0.87 (11)	1.51 (26)	1.15 (29)	0.29 (17)	0.15 (7)
$R_2 + R_3$	1.25 (15)	1.52 (20)	2.46 (42)	2.06 (52)	0.57 (33)	0.33 (16)
R_4 (FeIII)	0.43 (5)	0.03 (<1)	0.03 (<1)	0.04 (<1)	0.12 (7)	0.12 (5)
R_5 (SO_4^{2-})	6.55 (80)	6.19 (80)	3.40 (58)	1.91 (48)	0.82 (47)	1.10 (52)
Total	8.23	7.74	5.89	4.01	1.74	2.14

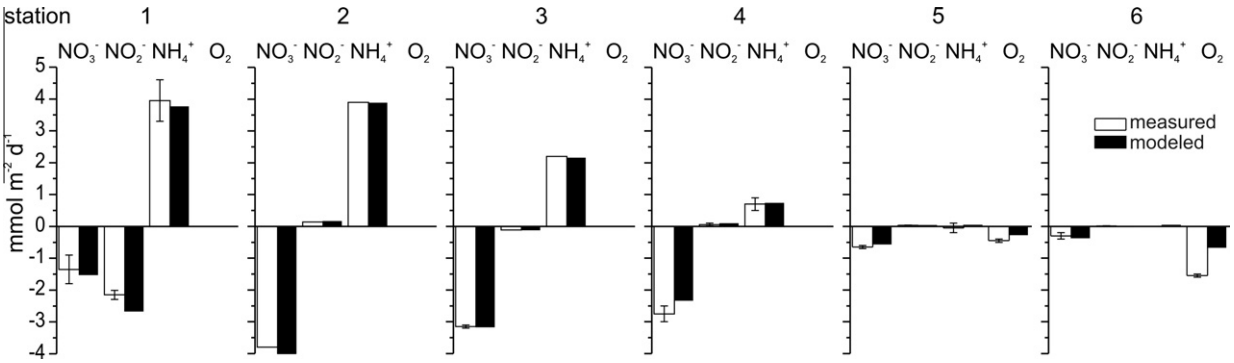

Fig. 4. Measured (empty columns) and modeled (filled columns) fluxes of DIN (mmol N m^{-2} d^{-1}) species and O_2 (mmol O_2 m^{-2} d^{-1}) across the sediment–water interface at each station. Error bars correspond to the measured minimum and maximum fluxes (at station 2 only one chamber was deployed). O_2 fluxes at stations 5 and 6 show the measured total oxygen uptake (TOU) in benthic chambers (Sommer et al., submitted for publication). N fluxes are from Sommer et al. (submitted for publication).

Iron reduction contributed only marginally to the overall POM degradation inside the OMZ (<1%) but accounted for 7% at the lower edge. Metal oxide reduction may account for up to 10–20% in highly bioturbated shelf sediments (Burdige, 2006), otherwise only 1% or less may be expected based on globally averaged studies (Thullner et al., 2009). The relatively high contribution from iron within the OMZ thus indicates that reactive iron fluxes are elevated in the area, perhaps by benthic release of ferrous iron on the shelf and oxidation to particulate ferric iron at the edges of the OMZ.

Porewater NO_3^- concentrations were depleted below the uppermost centimeter(s) at stations 2–5 (Fig. 3). Similarly, NO_2^- was generally <1 μM below the uppermost centimeter(s) (data not shown), yet was elevated at station 1 where measured bottom water concentrations were 11.5 μM (Table 3). However, at station 1 and 6, NO_3^- accumulated up to 10 μM below the surface layers. The reason for these anomalies is currently unclear, but may be due to deep bioirrigation at station 6 or experimental artifacts caused by ammonium oxidation as suggested by Woulds et al. (2009) who reported similar observations in the Pakistan margin OMZ. On the shelf there are further potential artifacts from the NO_3^- stored within vacuolated sulfur bacteria. At stations 1 and 3, surface NO_3^- concentrations in samples obtained using the porewater squeezing method exceeded 90–100 μM, whereas those using the centrifugation method or rhizons yielded much lower concentrations (<30 μM). Such elevated porewater NO_3^- concentrations have already been observed in *Thioploca* inhabited sediments off central Chile (Thamdrup and Canfield, 1996). A comparison of the different porewater extraction techniques indicates that the porewater squeezing and, to some extent also the centrifugation method, led to elevated NO_3^- concentrations by disrupting cells, whereas the use of rhizons appeared to be free of extraction artifacts (Fig. 3). Consequently, the elevated NO_3^- values at depths <10 cm were attributed to NO_3^- released from large sulfur bacteria and thus not representative of true porewater concentrations. Porewater squeezing was not used at station 2 and the significance of intracellular NO_3^- here is uncertain. In the absence of in situ NO_3^- data obtained from microbiosensors, we are cautious to draw any firm conclusions from our measured NO_3^- concentrations and these are not discussed further.

Nonetheless, the NO_3^- cycling is constrained using the benthic fluxes and we are confident that the modeled rates of denitrification are realistic. At the intermediate water depths (stations 3 and 4), NO_3^- (R_2) and NO_2^- (R_3) reduction accounted for 40–50% of POC degradation (Table 4), which is much higher than values of <10% predicted for the same water depth in normoxic settings (Thullner et al., 2009). In the absence of an upper oxic layer where aerobic respiration would inhibit denitrification, the denitrification

layer would be located at the sediment–water interface. The rate of denitrification would then be much less limited by diffusion of NO_3^- into the sediment since NO_3^- no longer has to traverse the aerobic zone. We hypothesize that this explains why up to half of POM is mineralized through this pathway. Despite anoxic bottom waters on the shelf, denitrification accounts for a lower, yet significant, fraction of carbon degradation (15–20%). We envisage that sediment clogging by microbial mats creates a barrier to NO_3^- diffusion and limits the efficiency of denitrifying bacteria at these depths.

4.2. Nitrogen turnover processes along the transect and their regulation

The fluxes of DIN species (NO_3^-, NO_2^-, NH_4^+) measured in the benthic landers were well reproduced by the model (Fig. 4). The overall magnitude of the fluxes decreased with increasing water depth which reflects lower organic matter reactivity and degradation rates. Accordingly, NH_4^+ effluxes were highest at the shallowest station 1 and decreased monotonously to almost zero at station 5 and 6. Nitrate fluxes were always directed into the sediment with the maximum uptake rate at station 2, whereas station 1 showed elevated nitrite uptake. This can be attributed to relatively low bottom water NO_3^- concentrations and high NO_2^- concentrations (Table 3). With regards to the net flux of DIN, the stations can be distinguished by region, that is, those where DIN was recycled in the sediments (fluxes of $NO_3^- + NO_2^- \approx NH_4^+$, stations 1 and 2) and those where the sediments were a sink for DIN (fluxes of $NO_3^- + NO_2^- > NH_4^+$, stations 3–6). These trends are discussed in more detail by Sommer et al. (submitted for publication).

The relative contributions of the various N turnover reactions to the measured fluxes along the 11°S transect are listed in Table 5 and an overview of the major pathways along the transect is shown in Fig. 5. In agreement with the trend for POM degradation and the benthic NH_4^+ effluxes, ammonification was highest at the shallowest station 1 and decreased with increasing water depth. Rates of POM degradation via nitrate and nitrite (R_2 and R_3, respectively) exhibited a peak at stations 3 and 4 (Fig. 5) where the relative contribution of these mineralization pathways was also highest (Table 4). The relatively lower rates of denitrification at stations 1 and 2, despite higher total POM degradation and the lack of O_2 have been explained as diffusion limitation of NO_3^- and NO_2^- from the bottom water. The predicted range of denitrification rates (R_2, R_3) was 0.2–2 mmol N m^{-2} d^{-1} and is consistent with rates measured at other low oxygen environments, for example, Concepción Bay (0.18–2.9 mmol N m^{-2} d^{-1}; Graco et al., 2001; Farías et al., 2004) and the Pakistan margin (0.07–3.68 mmol N m^{-2} d^{-1}; Schwartz et al., 2009).

In general, nitrification rates were low and could potentially supply <1.5% of NO_3^- or NO_2^- requirements for nitrate and nitrite reduction (Table 5). The major NO_3^- source for denitrification was thus identified as bottom water NO_3^-. The availability of NO_3^- may limit denitrification at the shallower stations 1–4 where bottom water NO_3^- concentrations were lower than those down slope (Table 3). In fact, nitrate reduction (R_2) was positively correlated with bottom water NO_3^- concentration at stations 1–4, but not at stations 5 and 6 where low rates were associated with high NO_3^- availability (Fig. 6). It is likely that aerobic respiration outcompetes denitrification for labile organic carbon here, thus limiting the amount of substrate which can be degraded by denitrification (Dale et al., 2011). The model by Middelburg et al. (1996) predicts similar tendencies for high-nutrient low-oxygen bottom waters.

Total DNRA exhibited highest rates at stations 1 and 2 (ca. 2.8 mmol m^{-2} d^{-1}) where DIN was recycled in the sediments leading to high release rates of NH_4^+ to the overlying water column (Table 5). With increasing water depth, DNRA rates decreased to zero. About 60% of total DNRA at station 1 occurred with NO_2^- (R_{10}). Simulated DNRA rates are consistent with minimum estimates from a simple mass balance for the upper 10 cm of the sediment column by Sommer et al. (submitted for publication), who calculated rates of 2.1–3.2 mmol N m^{-2} d^{-1} for station 1 and 2.9 mmol N m^{-2} d^{-1} for station 2. Within the OMZ, our DNRA rates (0.48–2.93 mmol N m^{-2} d^{-1}) were in the same range as found for Concepción Bay in summer (2.7–5 mmol N m^{-2} d^{-1}, Graco et al., 2001) and Laguna Madre/Baffin Bay (0.6–1.9 mmol N m^{-2} d^{-1}, An and Gardner, 2002) yet far lower than on the highly sulfidic sediments on the Namibian shelf colonized by *Thiomargarita* spp. (17 mmol N m^{-2} d^{-1}; Dale et al., 2009). A porewater sulfide budget (Supplementary material) revealed that DNRA removed 50–95% of the available free sulfide at stations 1–4 where bacterial mats were observed.

Table 5
N turnover rates (mmol N m^{-2} d^{-1}) across the transect. A 20% uncertainty is assigned to the rates (see Section 4.4).

Process	Station 1	Station 2	Station 3	Station 4	Station 5	Station 6
R_{AMF} ammonification	0.94	0.74	0.67	0.45	0.17	0.20
R_2 ($NO_3^- \rightarrow NO_2^-$)	0.35	1.31	1.90	1.83	0.55	0.36
R_3 ($NO_2^- \rightarrow N_2$)	1.44	1.16	2.02	1.53	0.39	0.20
R_6 nitrification ($NH_4^+ \rightarrow NO_2^-$)	0	0	0	0	2.2×10^{-4}	2.2×10^{-3}
R_7 nitrification ($NO_2^- \rightarrow NO_3^-$)	0	0	0	0	3.3×10^{-4}	5.6×10^{-4}
R_{11} NH_4^+ adsorption	6.9×10^{-3}	5.8×10^{-4}	8.5×10^{-4}	3.6×10^{-4}	7.2×10^{-5}	1.1×10^{-4}
R_9 DNRA ($NO_3^- \rightarrow NH_4^+$)	1.17	2.93	1.38	0.48	0	0
R_{10} DNRA ($NO_2^- \rightarrow NH_4^+$)	1.55	–	–	–	–	–
ΣDNRA	2.71	2.93	1.38	0.48	0	0
R_8 anammox ($NH_4^+ + NO_2^- \rightarrow N_2$)	0	0	0	0.43	0.28	0.33
% N_2 production by anammox	0	0	0	22	42	62

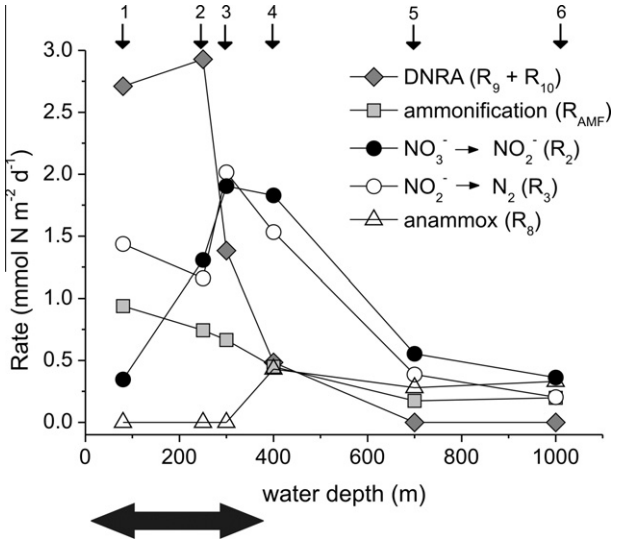

Fig. 5. Model-predicted depth-integrated rates of nitrogen turnover along the 11°S transect. Station numbers are indicated by the arrows at the top. The bottom arrow denotes the occurrence of bacterial mats (Mosch et al., 2010).

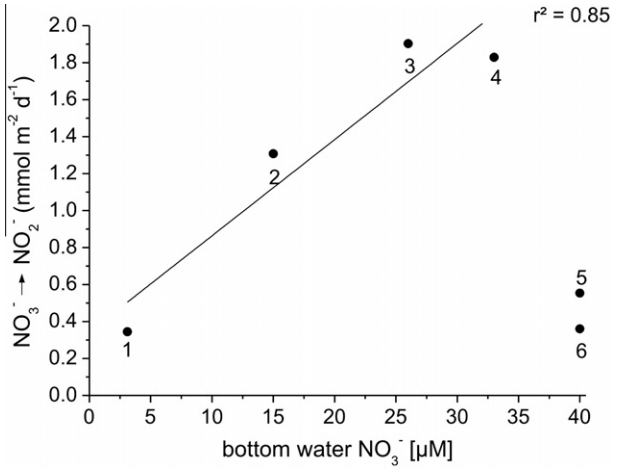

Fig. 6. Nitrate reduction (R_2) as a function of bottom water NO_3^- concentration for each station. The linear regression applies to stations 1–4 only.

Large sulfur bacteria compete with denitrifying bacteria for oxidized N. However, the sulfur bacteria may have a competitive edge in organic rich sediments where sulfide accumulates in the porewater. The balance between DNRA (favored at high TH_2S concentrations) and denitrification (favored at low TH_2S concentrations) may thus depend on the rate of sulfide sources (sulfate reduction) and sinks (oxidation and mineral sequestration) (An and Gardner, 2002; Dale et al., 2011). A positive linear correlation between the fraction of total NO_3^- consumed by DNRA and the modeled depth-integrated rate of sulfate reduction (Fig. 7) supports this idea. Moreover, *Thioploca* and *Beggiatoa* may move through the sediments at a rate of 10 cm per day (Jørgensen and Gallardo, 1999) which makes them more versatile to seek out NO_3^- than non-motile denitrifiers. They can also access bottom water NO_3^- and/or NO_2^- directly with their filaments and hence do not depend on NO_3^- supply by diffusion. Intracellular storage of NO_3^- (and potentially NO_2^-) within their vacuoles further allows them to thrive in areas of lower NO_3^- availability (Schulz and Jørgensen, 2001). Hence, because of these physiological adaptations, it is to be expected that DNRA accounts for the majority of the total NO_3^- uptake at the organic-rich shallower stations where bottom water NO_3^- availability was limited.

The data indicate that anammox only occurred at stations 4–6, with highest rates at station 4 (Fig. 5 and Table 5). Modeled depth-integrated anammox rates (0–0.43 mmol N m^{-2} d^{-1}) were consistent with measurements in sediments of the Skagerrak (0–0.6 mmol N m^{-2} d^{-1} from 0 to 1.5 cm; Dalsgaard and Thamdrup, 2002), the Washington margin (0.03–0.08 mmol N m^{-2} d^{-1}, Engström et al., 2009) and the North Atlantic (2.6×10^{-3}–0.06 mmol N m^{-2} d^{-1}; Trimmer and Nicholls, 2009). The regulation of anammox is ultimately dependent on the supply of NH_4^+ and NO_2^-. Despite the high rates of ammonification on the shelf, the absence of anammox at stations 1–3 likely results from the high demand for NO_2^- by denitrifiers which outcompete ammonium oxidizers for NO_2^- (cf. Dalsgaard et al., 2005; Risgaard–Petersen et al., 2005). At the deeper stations, NO_2^- supply directly from the water column was insufficient to support the simulated anammox rates. Furthermore, due to the low availability of O_2, only a small fraction of total NO_2^- turnover by anammox can be coupled to nitrification. In situ NO_3^- reduction to NO_2^- within the sediment via heterotrophic denitrification thus was the principal NO_2^- supply pathway for anammox. This pattern agrees with the analysis by Dale et al. (2011) who showed that anammox is most likely to be coupled to denitrification in sediments which are poorly ventilated and/or highly reactive and to nitrification in well ventilated sediments with lower fluxes of labile organic material. Other

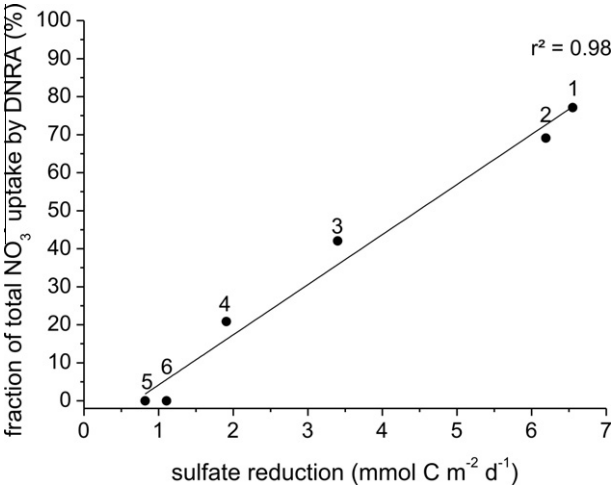

Fig. 7. Fraction of total benthic NO_3^- uptake by DNRA (%) as a function of the sulfate reduction rates. The solid denotes the linear fit to the data. Station numbers are indicated.

factors not considered here which are also potentially important with regards to anammox are inhibition of anammox by O_2 (Dalsgaard et al., 2005) and reduction of NO_3^- to NO_2^- by *Thioploca* (Prokopenko et al., 2006). Our model is able to explain the benthic fluxes without invoking these additional mechanisms.

4.3. Relative importance of denitrification, DNRA, and anammox in N cycling

Since DNRA retains DIN in the ecosystem while denitrification and anammox remove DIN, the channeling of oxidized N (NO_3^- and NO_2^-) into canonical denitrification and anammox versus DNRA determines the role of sediments as a recycling site or sink for DIN. The main sink for NO_3^- and NO_2^- in the sediments along the 11°S transect switched from DNRA ($\geqslant$65% of total uptake at stations 1 and 2) to coupled denitrification-anammox at stations 5 and 6 (Fig. 8) where microbial mats and DNRA were absent. Nitrification was negligible throughout (Table 5). For comparison, DNRA was responsible for 40% and 94% of total NO_3^- reduction in Concepción Bay sediments in spring and summer, respectively (Graco et al., 2001), and 70% at Boknis Eck (southwestern Baltic; Dale et al., 2011). Percentages in excess of 80% were observed in estuarine environments that receive high loads of nutrients (Jørgensen and Sørensen, 1985; Gilbert et al., 1997; Kim et al., 1997). Thus, at least at locations where large sulfur bacteria are present, NO_3^- uptake tends to be recycled to NH_4^+ at the expense of denitrifying processes. At stations 1 and 2, where DNRA governed both total N turnover (Fig. 5) and $NO_3^- + NO_2^-$ uptake (Fig. 8), DIN was recycled and large amounts of NH_4^+ were released by diffusion across the sediment–water interface (Fig. 4). The fate of NH_4^+ after being released from the Peruvian sediments is unknown, yet it may reach the euphotic zone and enhance primary production and the spread of the OMZ. This positive effect may be further exacerbated by the simultaneous release of excess phosphate and iron from the sediments that was also measured at the time of sampling (Noffke et al., 2010). At intermediate water depths (stations 3–6), where NO_3^- and NO_2^- uptake was mainly attributed to denitrification (Fig. 8) the sediments were a net sink for DIN (Fig. 4).

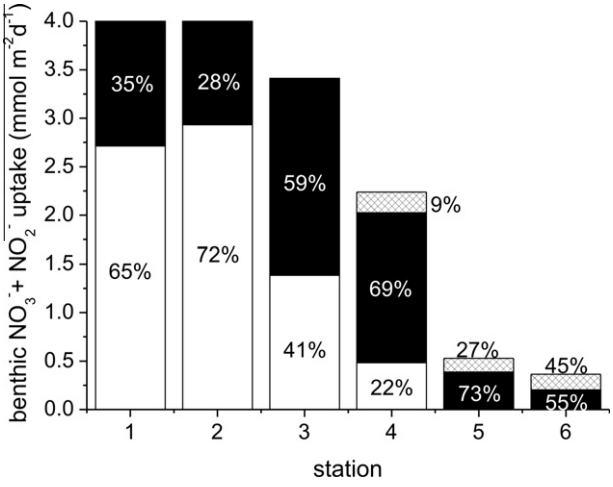

Fig. 8. Total model-predicted uptake of $NO_3^- + NO_2^-$ across the sediment–water interface (mmol N m^{-2} d^{-1}). The partitioning of the flux into DNRA (white), denitrification (black), and anammox (hashed) is given as percentage of the total flux.

Anammox accounted for up to 62% of N_2 production at the deepest station (Table 5), which is comparable to coastal sediments with oxic bottom waters in the Skaggerak (4–79%; Thamdrup and Dalsgaard, 2002; Engström et al., 2005) and coastal Greenland (1–35%; Rysgaard et al., 2004). Similar data for sediments underlying oxygen deficient environments are scarce, yet Glud et al. (2009) reported that anammox contributed 37% to the total N_2 production in the hypoxic Sagami Bay in Japan (55–60 μM O_2). In contrast to the absolute anammox rates, the relative importance of anammox in N_2 production increased with water depth from station 4 to 6 (Table 5). This negative relationship has been reported for a wide range of marine sediments (Thamdrup and Dalsgaard, 2002; Dalsgaard et al., 2005; Trimmer and Nicholls, 2009) and has been explained as increased coupling between anammox and nitrification because NO_2^- production by denitrification tends to decrease with increase water depth (Dale et al., 2011). In support of this thesis, the relative importance of anammox to total N_2 production was highest at stations 5 and 6 which had the lowest rates of denitrification and highest rates of nitrification (Table 5). Possible inhibition of anammox and denitrification on the shelf by sulfide (Joye, 2002; Dalsgaard et al., 2003) was not considered in our model since no free sulfide was observed in the upper sediment layers where anammox and denitrification take place (Fig. 3). The dominance of denitrification as the major sink in sediments underlying the OMZ is in contrast to water column studies on the Peru margin which observed that N cycling was dominated by anammox (Hamersley et al., 2007; Lam et al., 2009).

4.4. Potential importance of anammox on the shelf

The data analysis has shown that, under the assumptions imposed by the model, anammox was absent at stations 1–3 within the OMZ. However, despite the multiple constraints on the modeled turnover rates, this result remains to be corroborated with experimental evidence. The largest potential uncertainties in the anammox rate are introduced through the rate constant (k_8). The transport and physical parameters are reasonably well known and a realistic variability in their parameterization is likely to have less impact on anammox than the reaction kinetics. Thus, anammox may be occurring to some extent on the shelf, particularly at station 3 on the transition between the sediments dominated by DNRA and denitrification.

To test the potential importance of anammox at this station, we carried out a simple sensitivity analysis which consisted of re-running the baseline model using the lowest (3×10^9 M^{-1} $year^{-1}$) and highest (1.6×10^{10} M^{-1} $year^{-1}$) values of the anammox rate constant derived from the stations 4–6 where anammox was predicted. The lower values resulted in a rate of 1.0 mmol N m^{-2} d^{-1} (Table 6)

Table 6
Sensitivity study for station 3 to estimate the potential impact of anammox on NO_3^-, NO_2^- and N_2 fluxes across the sediment water interface and the depth integrated sulfate reduction rate. The standard run ($k_8 = 0$) is given in the first line of the table.

k_8 (M^{-1} $year^{-1}$)	Anammox (R_8) (mmol N m^{-2} d^{-1})	% N_2 production by anammox	NO_3^- flux	NO_2^- flux	N_2 flux	Sulfate reduction (R_4) (mmol SO_4^{2-} m^{-2} d^{-1})
			(% Change from standard run)			
0	0.0	0	–	–	–	1.7
3×10^9	1.0	29	+24	+92	+68	3.6
1.6×10^{10}	2.0	39	+58	+224	+156	5.3

which is about twice as high as simulated for station 4 (Table 5). The higher rate constant increases anammox to 2.0 mmol N m^{-2} d^{-1}. However, due to the highly coupled nature of the N cycle, increased anammox also enhances NO_3^- uptake, by 24% and 58% for the low and high rate constants, respectively. Furthermore, because anammox consumes NH_4^+, the higher rates lead to 2- to 3-fold increase in sulfate reduction (Table 6). This is a result of the procedure used to fit the modeled NH_4^+ values with the measured NH_4^+ pore water data (Eq. (5), Fig. 2B). Böning et al. (2004) reported a sulfate reduction rate of 1.9 mmol S m^{-2} d^{-1} for a site in close proximity to station 3. Although we recognize that spatial heterogeneity could account for a 2- to 3-fold increase in depth-integrated sulfate reduction rates, the close similarity of our modeled rate with those measured by Böning et al. (2004) plus the additional constraint of the measured NO_3^- flux indicates that the absence of anammox in the baseline simulation at station 3 is realistic.

Finally, it is worth noting that the sensitivity of NO_3^- and NO_2^- fluxes to anammox in Table 6 is much larger than the standard deviation of the measured fluxes (Fig. 4). Results were similar for the other N cycling reactions. This strongly restricts the leverage with which to vary the biogeochemical rates constant independently of one another. Furthermore, the measured fluxes must be consistent with the porewater profiles of TA, NH_4^+ and SO_4^{2-} which are a robust proxy for POM mineralization. Accordingly, and notwithstanding the usual inconvenience of local heterogeneity issues, the uncertainty in the modeled rates is determined by the uncertainty in the measured data (primarily the fluxes). At station 1 where the highest NH_4^+ release rates were measured, the precision in fluxes is around 20% (Fig. 4). Since NH_4^+ fluxes are the major constraint on the model (Eq. (5)), this value can be assumed to be reasonable estimate for the uncertainty in the simulated rates.

5. CONCLUSIONS

The dominant pathways and rates of benthic N cycling change dramatically through the Peruvian oxygen minimum zone (OMZ) at 11°S. DNRA governed total N turnover on the shelf and the upper slope (80–260 m water depth) where organic matter mineralization rates were high and bottom waters were depleted in O_2, NO_3^- and NO_2^-. These sediments represented a DIN recycling site, releasing large amounts of NH_4^+ by diffusion across the sediment–water interface. This may create a positive feedback with primary production and oxygen draw-down within the Peruvian OMZ. At greater water depths (>300 m), where organic carbon degradation decreased and bottom water NO_3^- concentrations increased, denitrification was the dominant pathway in the benthic N cycle and the sediments here were a net sink for DIN. Anammox was of minor importance on the shelf and upper slope but gained importance at water depths >400 m where it contributed up to 62% to total N_2 production at the deepest station.

Sediments underlying the oxygen deficient water of upwelling regions are commonly considered as sinks for DIN associated with high benthic NO_3^- uptake. However, this study shows that high benthic NO_3^- uptake rates in these environments are not always due to high rates of denitrification but may also result from DNRA. Consequently, the role of sediments underlying low oxygen waters as sinks for DIN should be revised and, furthermore, DNRA should be considered when interpreting benthic NO_3^- uptake in such settings. Models predict that OMZs are expanding due to climate change (Oschlies et al., 2008; Shaffer et al., 2009). Due consideration of DNRA versus denitrification with regards to the balance between net removal and recycling of DIN and the potential feedback on primary production is required to accurately predict the rate of spreading of OMZs.

Numerical transport-reaction modeling is an appropriate tool for the identification of pathways and quantification of rates of DIN turnover in marine surface sediments. The strength of the model developed here rests with the multiple constraints on N turnover, which include in situ benthic fluxes in addition to a suite of porewater data which allow the organic matter mineralization rates to be quantified. Both of these different sets of data must be coherent and consistent with one another when coupled to a set of reactions describing the major processes on N cycling on the Peruvian shelf. Our model parameterizations could be further verified using fluxes of stable N isotopes at sites both inside and outside the OMZ.

ACKNOWLEDGMENTS

We are grateful for the support of the crew of RV 'Meteor', leg M77-1/2 and B. Domeyer, M. Dibbern, R. Ebbinghaus and C. Ehlert for helping with the biogeochemical analyses. We also thank Jack Middelburg for the editorial handling and four anonymous reviewers for their constructive feedback which improved this manuscript. This work is a contribution of the Sonderforschungsbereich 754 "Climate – Biogeochemistry Interactions in the Tropical Ocean" (www.sfb754.de) which is supported by the Deutsche Forschungsgemeinschaft.

APPENDIX A. SUPPLEMENTARY DATA

Supplementary data associated with this article can be found, in the online version, at doi:10.1016/j.gca.2011.08.010.

REFERENCES

An S. M. and Gardner W. S. (2002) Dissimilatory nitrate reduction to ammonium (DNRA) as a nitrogen link, versus denitrification as a sink in a shallow estuary (Laguna Madre/Baffin Bay, Texas). *Mar. Ecol. Prog. Ser.* **237**, 41–50.

Berelson W. M., Hammond D. E. and Johnson K. S. (1987) Benthic fluxes and the cycling of biogenic silica and carbon in 2 Southern-California borderland basins. *Geochim. Cosmochim. Acta* **51**, 1345–1363.

Böning P., Brumsack H.-J., Böttcher M. E., Schnetger B., Kriete C., Kallmeyer J. and Borchers S. L. (2004) Geochemistry of Peruvian near-surface sediments. *Geochim. Cosmochim. Acta* **68**, 4429–4451.

Boudreau B. P. (1996) A method-of-lines code for carbon and nutrient diagenesis in aquatic sediments. *Comput. Geosci.* **22**, 479–496.

Boudreau B. P. (1997) *Diagenetic Models and Their Implementation*. Springer-Verlag.

Brandes J. A. and Devol A. H. (2002) A global marine-fixed nitrogen isotopic budget: Implications for holocene nitrogen cycling. *Global Biogeochem. Cycles* **16**, 1120.

Christensen P. B., Rysgaard S., Sloth N. P., Dalsgaard T. and Schwærter S. (2000) Sediment mineralization, nutrient fluxes, denitrification and dissimilatory nitrate reduction to ammonium in an estuarine fjord with sea cage trout farms. *Aquat. Microb. Ecol.* **21**, 73–84.

Codispoti L. A., Brandes J. A., Christensen J. P., Devol A. H., Naqvi S. W. A., Paerl H. W. and Yoshinari T. (2001) The oceanic fixed nitrogen and nitrous oxide budgets: moving targets as we enter the anthropocene? *Sci. Mar.* **65**, 85–105.

Dale A. W., Brüchert V., Alperin M. and Regnier P. (2009) An integrated sulfur isotope model for Namibian shelf sediments. *Geochim. Cosmochim. Acta* **73**, 1924–1944.

Dale A. W., Sommer S., Bohlen L., Treude T., Bertics V. J., Bange H. W., Pfannkuche O., Schorp T., Mattsdotter M. and Wallmann K. (2011) Rates and regulation of nitrogen cycling in seasonally-hypoxic sediments during winter (Boknis Eck, SW Baltic Sea): sensitivity to environmental variables. *Estuar. Coast. Shelf Sci.* Doi. 10.1016/j.ecss.2011.05.016.

Dalsgaard T. and Thamdrup B. (2002) Factors controlling anaerobic ammonium oxidation with nitrite in marine sediments. *Appl. Environ. Microb.* **68**, 3802–3808.

Dalsgaard T., Canfield D. E., Petersen J., Thamdrup B. and Acuña-González J. (2003) N_2 production by the anammox reaction in the anoxic water column of Golfo Dulce, Costa Rica. *Nature* **422**, 606–608.

Dalsgaard T., Thamdrup B. and Canfield D. E. (2005) Anaerobic ammonium oxidation (anammox) in the marine environment. *Res. Microbiol.* **156**, 457–464.

Devol A. H. and Christensen J. P. (1993) Benthic fluxes and nitrogen cycling in sediments of the continental-margin of the Eastern North Pacific. *J. Mar. Res.* **51**, 345–372.

Engström P., Dalsgaard T., Hulth S. and Aller R. C. (2005) Anaerobic ammonium oxidation by nitrite (anammox): Implications for N_2 production in coastal marine sediments. *Geochim. Cosmochim. Acta* **69**, 2057–2065.

Engström P., Penton C. R. and Devol A. H. (2009) Anaerobic ammonium oxidation in deep-sea sediments off the Washington margin. *Limnol. Oceanogr.* **54**, 1643–1652.

Falkowski P. G. (1997) Evolution of the nitrogen cycle and its influence on the biological sequestration of CO_2 in the ocean. *Nature* **387**, 272–275.

Farías L., Graco M. and Ulloa O. (2004) Temporal variability of nitrogen cycling in continental-shelf sediments of the upwelling ecosystem off central Chile. *Deep-Sea Res. Pt. II* **51**, 2491–2505.

Ferdelman T. G., Lee C., Pantoja S., Harder J., Bebout B. M. and Fossing H. (1997) Sulfate reduction and methanogenesis in a Thioploca-dominated sediment off the coast of Chile. *Geochim. Cosmochim. Acta* **61**, 3065–3079.

Fernández C., Farías L. and Alcaman M. E. (2009) Primary production and nitrogen regeneration processes in surface waters of the Peruvian upwelling system. *Prog. Oceanogr.* **83**, 159–168.

Fiedler P. C. and Talley L. D. (2006) Hydrography of the eastern tropical Pacific: a review. *Prog. Oceanogr.* **69**, 143–180.

Fossing H., Gallardo V. A., Jørgensen B. B., Hüttel M., Nielsen L. P., Schulz H., Canfield D. E., Forster S., Glud R. N., Gundersen J. K., Küver J., Ramsing N. B., Teske A., Thamdrup B. and Ulloa O. (1995) Concentration and transport of nitrate by the mat-forming sulfur bacterium Thioploca. *Nature* **374**, 713–715.

Froelich P., Arthur M., Burnett W., Deakin M., Hensley V., Jahnke R., Kaul L., Kim K.-H., Roe K., Soutar A. and Vathakanon C. (1988) Early diagenesis of organic matter in Peru continental margin sediments: phosphorite precipitation. *Mar. Geol.* **80**, 309–343.

Fuenzalida R., Schneider W., Garcés-Vargas J., Bravo L. and Lange C. (2009) Vertical and horizontal extension of the oxygen minimum zone in the eastern South Pacific Ocean. *Deep-Sea Res. Pt. II* **56**, 1027–1038.

Fulweiler R. W., Nixon S. W., Buckley B. A. and Granger S. L. (2007) Reversal of the net dinitrogen gas flux in coastal marine sediments. *Nature* **448**, 180–182.

Gallardo V. A. (1977) Large benthic microbial communities in sulphide biota under Peru–Chile subsurface countercurrent. *Nature* **268**, 331–332.

Gilbert F., Souchu P., Bianchi M. and Bonin P. (1997) Influence of shellfish farming activities on nitrification, nitrate reduction to ammonium and denitrification at the water–sediment interface of the Thau lagoon, France. *Mar. Ecol. Prog. Ser.* **151**, 143–153.

Glud R. N., Thamdrup B., Stahl H., Wenzhoefer F., Glud A., Nomaki H., Oguri K., Revsbech N. P. and Kitazatoe H. (2009) Nitrogen cycling in a deep ocean margin sediment (Sagami Bay, Japan). *Limnol. Oceanogr.* **54**, 723–734.

Graco M., Farías L., Molina V., Gutiérrez D. and Nielsen L. P. (2001) Massive developments of microbial mats following phytoplankton blooms in a naturally eutrophic bay: implications for nitrogen cycling. *Limnol. Oceanogr.* **46**, 821–832.

Grasshoff K., Ehrhardt M. and Kremling K. (1999) *Methods of Seawater Analysis*. Wiley-VCH, Weinheim.

Gruber N. (2004) The dynamics of the marine nitrogen cycle and its influence on the atmospheric CO_2 variations. In *The Ocean Carbon Cycle and Climate* (eds. Follows M. and Oguz T.). NATO ASI Series. pp. 97–148.

Gruber N. and Sarmiento J. L. (1997) Global patterns of marine nitrogen fixation and denitrification. *Global Biogeochem. Cycles* **11**, 235–266.

Gutiérrez D., Enriquez E., Purca S., Quipúzcoa L., Marquina R., Flores G. and Graco M. (2008) Oxygenation episodes on the continental shelf of central Peru: remote forcing and benthic ecosystem response. *Prog. Oceanogr.* **79**, 177–189.

Gutiérrez D., Sifeddine A., Field D. B., Ortlieb L., Vargas G., Chávez F. P., Velazco F., Ferreira V., Tapia P., Salvatteci R., Boucher H., Morales M. C., Valdés J., Reyss J. L., Campusano

A., Boussafir M., Mandeng-Yogo M., García M. and Baumgartner T. (2009) Rapid reorganization in ocean biogeochemistry off Peru towards the end of the Little Ice Age. *Biogeosciences* **6**, 835–848.

Hamersley M. R., Lavik G., Woebken D., Rattray J. E., Lam P., Hopmans E. C., Damsté J. S. S., Krüger S., Graco M., Gutiérrez D. and Kuypers M. M. M. (2007) Anaerobic ammonium oxidation in the Peruvian oxygen minimum zone. *Limnol. Oceanogr.* **52**, 923–933.

Hamme R. C. and Emerson S. R. (2004) The solubility of neon, nitrogen and argon in distilled water and seawater. *Deep-Sea Res. Pt. I* **51**, 1517–1528.

Hartnett H. E. and Devol A. H. (2003) Role of a strong oxygen-deficient zone in the preservation and degradation of organic matter: a carbon budget for the continental margins of northwest Mexico and Washington State. *Geochim. Cosmochim. Acta* **67**, 247–264.

Henrichs S. M. and Farrington J. W. (1984) Peru upwelling region sediments near 15°S. 1: Remineralization and accumulation of organic matter. *Limnol. Oceanogr.* **29**, 1–19.

Ingall E. and Jahnke R. (1994) Evidence for enhanced phosphorus regeneration from marine-sediments overlain by oxygen depleted waters. *Geochim. Cosmochim. Acta* **58**, 2571–2575.

Ivanenkov V. N. and Lyakhin Y. (1978) Determination of total alkalinity in seawater. In *Methods of Hydrochemical Investigations in the Ocean* (eds. O. K. Bordovsky and V. N. Ivanenkov). Nauka Publishing House, pp. 110–114.

Jørgensen B. B. and Gallardo V. A. (1999) *Thioploca* spp: filamentous sulfur bacteria with nitrate vacuoles. *FEMS Microbiol. Ecol.* **28**, 301–313.

Jørgensen B. B., Nelson D. (2004) Sulfide oxidation in marine sediments: geochemistry meets microbiology. In *Sulfur Biogeochemistry: Past and Present* (eds. J. P. Amend, T. W. Edwards and K. J. E. Lyons). Geological Society of America, Special Paper 379. pp. 63–81.

Jørgensen B. B. and Sørensen J. (1985) Seasonal cycles of O_2, NO_3- and SO_4^2-reduction in estuarine sediments – the significance of an NO_3 – reduction maximum in spring. *Mar. Ecol. Prog. Ser.* **24**, 65–74.

Jørgensen B. B., Böttcher M. E., Luschen H., Neretin L. N. and Volkov I. I. (2004) Anaerobic methane oxidation and a deep H_2S sink generate isotopically heavy sulfides in black sea sediments. *Geochim. Cosmochim. Acta* **68**, 2095–2118.

Joye S. B. (2002) Denitrification in the marine environment. In *Encyclopedia of Environmental Microbiology* (ed. G. Collins). Wiley, New York, pp. 1010–1019.

Kessler W. S. (2006) The circulation of the eastern tropical Pacific: a review. *Prog. Oceanogr.* **69**, 181–217.

Kim D., Matsuda O. and Yamamoto T. (1997) Nitrification, denitrification and nitrate reduction rates in the sediment of Hiroshima Bay, Japan. *J. Oceanogr.* **53**, 317–324.

Krissek L. A., Scheidegger K. F. and Kulm L. D. (1980) Surface sediments of the Peru–Chile continental-margin and the Nazca plate. *Geol. Soc. Am. Bull.* **91**, 321–331.

Kuypers M. M. M., Sliekers A. O., Lavik G., Schmid M., Jørgensen B. B., Kuenen J. G., Damsté J. S. S., Strous M. and Jetten M. S. M. (2003) Anaerobic ammonium oxidation by anammox bacteria in the Black Sea. *Nature* **422**, 608–611.

Lam P. and Kuypers M. M. M. (2011) Microbial nitrogen cycling processes in oxygen minimum zones. *Annu. Rev. Mar. Sci.* **3**, 317–345.

Lam P., Lavik G., Jensen M. M., van de Vossenberg J., Schmid M., Woebken D., Dimitri G., Amann R., Jetten M. S. M. and Kuypers M. M. M. (2009) Revising the nitrogen cycle in the Peruvian oxygen minimum zone. *Proc. Natl. Acad. Sci. USA* **106**, 4752–4757.

Levin L., Gutiérrez D., Rathburn A., Neira C., Sellanes J., Muñoz P., Gallardo V. and Salamanca M. (2002) Benthic processes on the Peru margin: a transect across the oxygen minimum zone during the 1997–98 El Nino. *Prog. Oceanogr.* **53**, 1–27.

Middelburg J. J., Soetaert K., Herman P. M. J. and Heip C. H. R. (1996) Denitrification in marine sediments: a model study. *Global Biogeochem. Cycles* **10**, 661–673.

Morales C. E., Hormazábal S. E. and Blanco J. L. (1999) Interannual variability in the mesoscale distribution of the depth of the upper boundary of the oxygen minimum layer off northern Chile (18–24S): implications for the pelagic system and biogeochemical cycling. *J. Mar. Res.* **57**, 909–932.

Morse J. W. and Morin J. (2005) Ammonium interaction with coastal marine sediments: influence of redox conditions on K^*. *Mar. Chem.* **95**, 107–112.

Mosch T., Sommer S., Pfannkuche O. and Wallmann K. (2010) Habitat Mapping in the Peruvian OMZ. *Eos Trans. AGU, 91*(26), Ocean Sci. Meet. Suppl., #BO35C-08 (abstr.).

Niggemann J., Ferdelman T. G., Lomstein B. A., Kallmeyer J. and Schubert C. J. (2007) How depositional conditions control input, composition, and degradation of organic matter in sediments from the chilean coastal upwelling region. *Geochim. Cosmochim. Acta* **71**, 1513–1527.

Noffke A., Hensen C., Sommer S., Scholz F. and Wallmann K. (2010) Benthic fluxes of iron, phosphate and silicate across the Peruvian Oxygen Minimum Zone. *Eos Trans. AGU, 91*(26), Ocean Sci. Meet. Suppl., #BO35C-09 (abstr.).

Oschlies A., Schulz K. G., Riebesell U. and Schmittner A. (2008) Simulated 21st century's increase in oceanic suboxia by CO_2-enhanced biotic carbon export. *Global Biogeochem. Cycles* **22**, GB4008.

Otte S., Kuenen J. G., Nielsen L. P., Paerl H. W., Zopfi J., Schulz H. N., Teske A., Strotmann B., Gallardo V. A. and Jørgensen B. B. (1999) Nitrogen, carbon, and sulfur metabolism in natural Thioploca samples. *Appl. Environmental. Microb.* **65**, 3148–3157.

Pennington J. T., Mahoney K. L., Kuwahara V. S., Kolber D. D., Calienes R. and Chavez F. P. (2006) Primary production in the eastern tropical Pacific: a review. *Prog. Oceanogr.* **69**, 285–317.

Poulton S. W. and Raiswell R. (2002) The low-temperature geochemical cycle of iron: from continental fluxes to marine sediment deposition. *Am. J. Sci.* **302**, 774–805.

Preisler A., de Beer D., Lichtschlag A., Lavik G., Boetius A. and Jørgensen B. B. (2007) Biological and chemical sulfide oxidation in a Beggiatoa inhabited marine sediment. *ISME J.* **1**, 341–353.

Prokopenko M. G., Hammond D. E., Berelson W. M., Bernhard J. M., Stott L. and Douglas R. (2006) Nitrogen cycling in the sediments of Santa Barbara basin and Eastern Subtropical North Pacific: nitrogen isotopes, diagenesis and possible chemosymbiosis between two lithotrophs (Thioploca and Anammox) –"riding on a glider". *Earth Planet. Sci. Lett.* **242**, 186–204.

Reimers C. and Suess E. (1983) Spatial and temporal patterns of organic matter accumulation on the Peru continental margin. In *Coastal Upwelling its Sediment Record. Part B: Sedimentary Records of Ancient Coastal Upwelling* (eds. J. Thiede and E. Suess). Plenum Press, pp. 311–346.

Risgaard-Petersen N., Meyer R. L. and Revsbech N. P. (2005) Denitrification and anaerobic ammonium oxidation in sediments: effects of microphytobenthos and NO_3^-. *Aquat. Microb. Ecol.* **40**, 67–76.

Rowe G. T. and Howarth R. (1985) Early diagenesis of organic matter in sediments off the coast of Peru. *Deep-Sea Res. Pt. A* **32**, 43–55.

Rysgaard S., Glud R. N., Risgaard-Petersen N. and Dalsgaard T. (2004) Denitrification and anammox activity in Arctic marine sediments. *Limnol. Oceanogr.* **49**, 1493–1502.

Sarbas B. and Nohl U. (2009) The GEOROC database – a decade of "online geochemistry". *Geochim. Cosmochim. Acta* **73**, A1158.

Schulz H. N. and Jørgensen B. B. (2001) Big bacteria. *Annu. Rev. Microbiol.* **55**, 105–137.

Schwartz M. C., Woulds C. and Cowie G. L. (2009) Sedimentary denitrification rates across the Arabian Sea oxygen minimum zone. *Deep-Sea Res. Pt. II* **56**, 324–332.

Shaffer G., Olsen S. M. and Pedersen J. O. P. (2009) Long-term ocean oxygen depletion in response to carbon dioxide emissions from fossil fuels. *Nat. Geosci.* **2**, 105–109.

Sifeddine A., Gutiérrez D., Ortlieb L., Boucher H., Velazco F., Field D., Vargas G., Boussafir M., Salvatteci R., Ferreira V., Garcia M., Valdés J., Caquineau S., Yogo M. M., Cetin F., Solis J., Soler P. and Baumgartner T. (2008) Laminated sediments from the central Peruvian continental slope: a 500 year record of upwelling system productivity, terrestrial runoff and redox conditions. *Progr. Oceanogr.* **79**, 190–197.

Silva N., Rojas N. and Fedele A. (2009) Water masses in the humboldt current system: properties, distribution, and the nitrate deficit as a chemical water mass tracer for Equatorial Subsurface Water off Chile. *Deep-Sea Res. Pt. II* **56**, 992–1008.

Sommer S., Linke P., Pfannkuche O., Niemann H. and Treude T. (2010) Benthic respiration in a seep habitat dominated by dense beds of ampharetid polychaetes at the Hikurangi Margin (New Zealand). *Mar. Geol.* **272**, 223–232.

Sommer S., Bohlen L., Dale, A. W., Pfannkuche O. and Wallmann K. (submitted for publication) Nitrogen fluxes across Peruvian oxygen minimum zone surface sediments – the potential significance of DNRA. *Global Biogeochem. Cycles*.

Stramma L., Johnson G. C., Sprintall J. and Mohrholz V. (2008) Expanding oxygen-minimum zones in the tropical oceans. *Science* **320**, 655–658.

Straub K. L., Benz M., Schink B. and Widdel F. (1996) Anaerobic, nitrate-dependent microbial oxidation of ferrous iron. *Appl. Environ. Microb.* **62**, 1458–1460.

Suess E., Kulm L. D. and Killingley J. S. (1987) Coastal upwelling and a history of organic-rich mudstone deposition off Peru. In *Marine Petroleum Source Rocks* (eds. Brooks J. and Fleet A.J.). Geological Society. pp. 181–197.

Thamdrup B. and Canfield D. E. (1996) Pathways of carbon oxidation in continental margin sediments off central Chile. *Limnol. Oceanogr.* **41**, 1629–1650.

Thamdrup B. and Dalsgaard T. (2002) Production of N_2 through anaerobic ammonium oxidation coupled to nitrate reduction in marine sediments. *Appl. Environ. Microb.* **68**, 1312–1318.

Thauer R. K., Jungermann K. and Decker K. (1977) Energy-conservation in chemotrophic anaerobic bacteria. *Bacteriol. Rev.* **41**, 100–180.

Thullner, M., Dale, A. W. and Regnier P. (2009) Global-scale quantification of mineralization pathways in marine sediments: a reaction-transport modeling approach. *Geochem. Geophys. Geosyst*. **10**, Q10012, doi:10.1029/2009GC002484.

Trimmer M. and Nicholls J. C. (2009) Production of nitrogen gas via anammox and denitrification in intact sediment cores along a continental shelf to slope transect in the North Atlantic. *Limnol. Oceanogr.* **54**, 577–589.

Van Cappellen P. and Ingall E. D. (1994) Benthic phosphorus regeneration, net primary production, and ocean anoxia: a model of the coupled marine biogeochemical cycles of carbon and phosphorus. *Paleoceanography* **9**, 677–692.

Van Cappellen P. and Wang Y. (1996) Cycling of iron and manganese in surface sediments; a general theory for the coupled transport and reaction of carbon, oxygen, nitrogen, sulfur, iron, and manganese. *Am. J. Sci.* **296**, 197–243.

Wallmann K. (2010). Phosphorus imbalance in the global ocean? *Global Biogeochem. Cycles* **24**, GB4030.

Wallmann K., Aloisi G., Haeckel M., Tishchenko P., Pavlova G., Greinert J., Kutterolf S. and Eisenhauer A. (2008) Silicate weathering in anoxic marine sediments. *Geochim. Cosmochim. Acta* **72**, 2895–2918.

Wolf-Gladrow D. A., Zeebe R. E., Klaas C., Körtzinger A. and Dickson A. G. (2007) Total alkalinity: the explicit conservative expression and its application to biogeochemical processes. *Mar. Chem.* **106**, 287–300.

Woulds C., Schwartz M.C., Brand T., Cowie G., Law G. and Mowbray S. (2009). Porewater nutrient concentrations and benthic nutrient fluxes across the Pakistan margin OMZ. *Deep-Sea Res. II* **56**, 333–346.

Zopfi J., Kjær T., Nielsen L. P. and Jørgensen B. B. (2001) Ecology of *Thioploca* spp.: nitrate and sulfur storage in relation to chemical microgradients and influence of *Thioploca* spp. on the sedimentary nitrogen cycle. *Appl. Environ. Microb.* **67**, 5530–5537.

Zuta S. and Guillén O. (1970). , pp. 161–323.

Associate editor: Jack J. Middelburg